

Probing Broadband Spectral Energy Distribution and Variability of Mrk 501 in the low flux state

Javaid Tantry^{a,**}, Zahir Shah^{b,**}, Ranjeev Misra^c, Naseer Iqbal^a, Sikandar Akbar^a

^a*Department of Physics University of Kashmir Srinagar 190006 India*

^b*Department of Physics Central University of Kashmir Ganderbal-19113 India*

^c*Inter-University Centre for Astronomy and Astrophysics Post Bag 4 Ganeshkhind Pune-411007 India*

Abstract

We conducted a multi-wavelength analysis of the blazar Mrk 501, utilizing observations from *AstroSat* (SXT, LAXPC), *Swift-UVOT*, and *Fermi-LAT* during the period August 15, 2016 to March 27, 2022. The resulting multi-wavelength light curve revealed relatively low activity of the source across the electromagnetic spectrum. Notably, logparabola and broken power-law models provided a better fit to the joint X-ray spectra from *AstroSat-SXT/LAXPC* instruments compared to the power-law model. During the low activity state, the source showed the characteristic harder when brighter trend at the X-ray energies. To gain insights into underlying physical processes responsible for the broadband emission, we performed a detailed broadband spectral analysis using the convolved one-zone leptonic model with different forms of particle distributions such as logparabola (LP), broken power-law (BPL), power-law model with maximum energy (ξ_{max}), and energy-dependent acceleration (EDA) models. Our analysis revealed similar reduced- χ^2 values for the four particle distributions. The LP and EDA models exhibited the lowest jet powers. The correlation analyses conducted for the LP and BPL models revealed that there is a positive correlation between jet power and bulk Lorentz factor. Specifically, in the LP model, jet power proved independent of γ_{min} , whereas in the broken power-law model, jet power decreased with an increase in γ_{min} . The jet power in the LP/EDA particle distribution is nearly 10 percent of the Eddington luminosity of a $10^7 M_\odot$ black hole. This result suggests that the jet could potentially be fueled by accretion processes.

Keywords: galaxies: active, galaxies: BL Lacertae objects: Mrk 501, jets, radiation mechanisms: non-thermal - gamma-rays, galaxies: Jets; Active

1. Introduction

Blazars are subclass of active galactic nuclei (AGN) with relativistic jet pointing close to the line of sight of an observer (Blandford and Rees, 1978; Urry and Padovani, 1995). They are characterized by strong γ -ray emissions, high degree polarization, rapid variability and nonthermal spectrum extending from radio to γ -ray energies (Wills et al., 1992; Ackermann and et al., 2015; Fan et al., 2018a; Ajello et al., 2020; Zhang et al., 2021). The close pointing of relativistic jet results in relativistic beaming which further amplifies the observational properties (Blandford and Rees, 1978; Urry and Padovani, 1995; Böttcher et al., 2003). On the basis of their spectral features, blazars are broadly identified as flat-spectrum radio quasars (FSRQs) and BL Lacertae objects (BL Lacs). FSRQs exhibit strong emission line features in their optical spectrum, while BL Lacs display weak or no emission line features (Urry and Padovani, 1995).

The broadband spectral energy distribution (SED) of blazars exhibits double humped shape and the emission extends from

radio to GeV/TeV energies. According to the leptonic model, this broadband emission can be attributed to the synchrotron and inverse-Compton (IC) processes. The low-energy hump, peaking in the Optical/UV/X-ray energy is produced by the synchrotron process, while the high energy hump peaking in the γ -ray band, is mainly explained by IC scattering of low-energy photons (Urry and Mushotzky, 1982; Blandford and Levinson, 1995). The seed photons for IC scattering can be either synchrotron photons leading to the synchrotron self-Compton process (SSC; Jones et al., 1974; Shah et al., 2017), or photons entering external to the jet called external Compton process (EC; Dermer et al., 1992; Sikora et al., 1994). Alternatively, the high energy emission from blazars can also be explained through a hadronic process initiated by the relativistic protons, involving the proton-synchrotron processes and pion production processes (Mannheim and Biermann, 1992; Mücke and Protheroe, 2001). Based on the peak frequency of the synchrotron component, BL Lacs are further divided into low-energy peaked BL Lac (LBL; $\nu_p < 10^{14}$ Hz), intermediate-energy peaked BL lacs (IBL; $10^{14} < \nu_p < 10^{15}$) and high-energy peaked BL Lacs (HBL; $\nu_p > 10^{15}$) (Padovani and Giommi, 1995).

Mrk 501 is a BL Lac object at a redshift $z \sim 0.034$. It is one of the nearest bright HBL source in X-rays (Massaro et al., 2004). The source was detected at the very high energy (VHE) band by the Whipple observatory in 1995 and became the second

*Corresponding author: Javaid Tantry

**Corresponding author: Zahir Shah

Email addresses: javaitantray9@gmail.com (Javaid Tantry), shahzahir4@gmail.com (Zahir Shah)

extragalactic source detected in the VHE band (Quinn et al., 1996). The source underwent a strong VHE flare in 1997 with peak flux upto ten times the Crab nebula flux and flux-doubling timescales of half a day (Aharonian et al., 1999). The VHE flare was accompanied by the correlated emissions in the X-ray band with a very hard X-ray spectrum (Pian et al., 1998). It showed TeV flare again in June 1998, during which the peak of the synchrotron component shifted to high energy ≥ 50 keV (Sambruna and et al., 2000). Paneque (2007) showed that the VHE flux of the source varied by an order of magnitude during the MAGIC campaign in May–July 2005, with the flux doubling timescale of ~ 2 minutes.

In the X-ray band, Rossi X-Ray Timing Explorer (RXTE) has observed remarkable X-ray variability from the source (Gliozzi et al., 2006). Later *Swift*-XRT observations showed a powerful and prolonged X-ray activity from the source during March–October 2014 (Kapanadze et al., 2017). This long outburst was reported to be superimposed with several shorter flares. Moreover, during a strong flaring event, the X-ray spectral evolution demonstrated a harder when brighter pattern with a spectral index harder than 1.70. The source showed another long flare in 2021, a detailed X-ray timing and spectral analysis of this outburst was carried out by Kapanadze et al. (2023). During this period, the X-ray spectrum was hard and showed significant curvature features.

Being a strong variable source, it has been extensively studied in the last three decades. Several multi-wavelength studies of the source have been carried out to understand the physical processes responsible for the flux variation (Pian et al., 1998; Sambruna and et al., 2000; Abdo et al., 2011). Recently, Abe et al. (2024) carried the first multi-wavelength analysis of Mrk 501 along with the simultaneous X-ray polarisation data from the Imaging X-ray Polarimetry Explorer (IXPE). The authors explained the variation in the three IXPE pointing observation due to the change in the size of emission region or variation in the magnetic field. The broadband emission of Mrk 501 during the low flux state (2017 – 2020) was studied by Abe et al. (2023). During this period, a historical low activity is reported in Mrk 501 in the X-ray and VHE γ -ray bands. Such observations helped to unravel the baseline emission from the source. The authors showed that the multi-wavelength light curves are significantly correlated, supporting the leptonic scenario for the broadband emission. The broadband SED during the high and low flux states are adequately modeled with a one-zone leptonic model involving synchrotron and SSC processes (Ahnen et al., 2018; Abe et al., 2023). Similarly, a one-zone SSC model described the broadband SED of Mrk 501 during an extreme X-ray outburst in July 2014 (MAGIC Collaboration et al., 2020). The SEDs in different flux states were reproduced with the variation in the break energy, magnetic field, and spectral shapes of the particle distribution. Especially, on the day of peak X-ray flux, an unusually narrow feature was observed in the VHE spectrum. This feature, inconsistent with classical particle distribution forms, was best described by a logparabola with an additional narrow component, challenging conventional models at TeV energies (MAGIC Collaboration et al., 2020). These results suggest that

despite numerous studies on the source, the nature of this object is still not well understood.

Blazars represent extremely powerful sources within the extra-galactic universe. Their emission is mainly dominated by the non-thermal emission from the relativistic jets. Theoretical models suggest that these jets originate from a spinning black hole, with their power linked either to the spin and mass of the black hole (Blandford and Znajek, 1977) or to the black hole spin and the angular velocity (Moderski and Sikora, 1996; Ghosh and Abramowicz, 1997). In the case of blazars, the jet power is usually estimated through broadband SED modeling. Understanding the physical processes behind the extreme emission from the relativistic jet remains the main research area in blazars. Several multi-wavelength (MWL) studies have been carried out to understand the emission process and to infer the physical parameters playing a role in the jet emission (Zhang and Böttcher, 2013; Zhang et al., 2014; Fan et al., 2018b). For example, Shah et al. (2017) used the approximate analytical expressions for synchrotron, SSC and EC processes to constraint the high energy emission mechanism and source of seed photons for the IC process. Additionally, Ghisellini et al. (2005) examined the physical processes behind the high-energy emission from blazars by investigating the correlations between the jet power and other observed properties such as the γ -ray brightness and the synchrotron luminosity. We conduct a multi-wavelength study of Mrk 501 by using the broadband observations from *AstroSat*, *Swift*, and *Fermi* Telescopes. Within the framework of one-zone leptonic model, we examined the implications on the jet energetics by using different forms of particle distribution. Particularly, we constrained the underlying particle distribution by obtaining the minimum jet power condition. The correlation analyses are carried out between the jet power and the underlying physical parameters to check the consistency of the particle distributions. Recently, Bora et al. (2024) studied the jet power of Mrk 501 during its low state, using multi-wavelength data that was not strictly simultaneous, with typical differences of a few hours between *Swift* and *NuSTAR* observations. In contrast, our work utilized the simultaneous multi-wavelength capabilities of *AstroSat*'s SXT and LAXPC instruments in the broad range of X-rays, providing comprehensive coverage of the synchrotron component within the broadband SED (Ahnen et al., 2017). The high exposure time with *AstroSat* provides a significantly better quality spectrum, enabling verification of Bora et al. (2024) results using independent data. Furthermore, longer *AstroSat* observations allow us to do a detailed temporal and spectral analysis in X-rays, which was not performed in Bora et al. (2024). This work is structured in the following ways: Section §2 provides the details of observation and data processing techniques. In section §3, we report the temporal and spectral results of Mrk 501 using the *AstroSat* observations. Section §4 contains the multi-wavelength light curve and fractional variability results. The broadband spectral analysis results are presented in Section §5. Finally, the paper concludes with a summary and discussion in Section §6.

2. Observations and Data reduction

2.1. AstroSat

AstroSat being a multi-wavelength observatory consisting of Ultra-violet Imaging Telescope (UVIT; Tandon et al., 2017), Soft X-ray Focusing Telescope (SXT; Singh et al., 2017), Large Area X-ray Proportional Counter (LAXPC; Yadav et al., 2016), and Cadmium Zinc Telluride Imager (CZTI; Rao et al., 2017). It permits the simultaneous observation of the source at UV, soft X-ray, and hard X-ray energies. *AstroSat* conducted five observations of Mrk 501 during the period MJD 57615.2 – 59666, we identified these observations as S1 (57615.2 – 57615.9), S2 (58594.9 – 58596.2), S3 (58910.3 – 58912), S4 (58934.5 – 58939.8), and S5 (59662.3 – 59665.8). The details of *AstroSat* observations of Mrk 501 are given in Table 1. In this section, we provide the details of the data reduction procedures applied to the observations made by the SXT and LAXPC instruments.

2.1.1. SXT DATA

SXT onboard *AstroSat* is an X-ray imaging telescope sensitive in the energy range 0.3 – 8.0 keV with an effective area of $\sim 90 \text{ cm}^2$ at 1.5 keV (Singh et al., 2017). It is designed to provide soft X-ray images, light curves and spectra in the energy range 0.3 – 8.0 keV. During the time period MJD 57615 – 59666, Mrk 501 was observed in photon counting (PC) mode. We processed the level-1 data in each orbit to level-2 data by using SXTPipeline version AS1SXTLevel2-1.4a released on January 6, 2017. In order to obtain a single cleaned event file, we merge the level-2 data of all orbits by using the SXTEVTMERGER tool. Science products (light curve and spectra) were generated from the merged event files using XSELECT (V2.4d) package which is available in the HEASoft software. A circular region of 15' radius centered on the source was used to extract source spectra and light curve, the selected circular region covers 90% of the source photons. The spectral analysis was carried out by using the background spectrum SkyBkg_comb_EL3p5_C1_Rd16p0v01.pha, and response matrix file (RMF) “sxt_pcmat_g0to12.rmf” provided by the SXT POC team. Further, we used an off-axis auxiliary response file (ARF) generated using SXT ARF generation tool¹. To ensure the optimal number of counts per bin, we have used *ftgrouppha* package available in HeaSoft software (Kaastra and Bleeker, 2016).

2.1.2. LAXPC DATA

The LAXPC is another payload onboard *AstroSat*, it consists of three co-aligned identical non-imaging proportional counters namely LAXPC10, LAXPC20, and LAXPC30 (Yadav et al., 2016). It has a total effective area of 6000 cm^2 at 15 keV. The LAXPC detectors can observe photons with a time resolution of $\sim 10 \mu\text{s}$. LAXPC has the ability to perform observations

in a broad range of energies 3.0 – 80.0 keV. The detailed information about the LAXPC instrument is provided as (Roy et al., 2016; Yadav et al., 2016), and (Agrawal et al., 2017). Due to gain instability issues with LAXPC10 and LAXPC30 being officially shut down, we have only used data from LAXPC20 in our work. The processing of Level-1 data and the extraction of light curves/spectra were done with the software package LAXPCSOFT. Since blazars are faint sources for LAXPC, we used the scheme of faint source algorithm which is implemented as a part of LAXPCSOFT for extracting the light curves and spectra. The background subtraction was done by the standard FTool lcmath package. We restricted the temporal analysis to the energy range 3.0 – 30.0 keV and spectral analysis to the energy range 4.0 – 17.0 keV, since the background dominates the source spectrum above these energies.

2.2. Swift-UVOT

Swift is a space-based observatory equipped with Burst Alert Telescope (BAT), X-ray Telescope (XRT) (Barthelmy et al., 2005; Burrows et al., 2005) and Ultraviolet/Optical Telescope (UVOT) (Roming et al., 2005). It observes the sources in the sky at hard X-ray bands, soft X-ray bands, ultraviolet, and optical bands. *Swift*-UVOT provides Optical/UV data with V, B, U, W1, M2, and W2 filters. Notably, during most *AstroSat* observations of Mrk 501, *Swift* also observed the source simultaneously. The *Swift*-UVOT data of Mrk 501 are available in all six filters, except during the period MJD 57614 – 57615, where only V-filter observations are available. We retrieved the data of Mrk 501 from HEASARC Archive and processed it into scientific products using the HEASoft packages namely *UVOTSOURCE* and *UVOTIMSUM*. The *UVOTSOURCE* package was used to process the images, while the *UVOTIMSUM* package was used to add multiple images in the filters. The photometry of the source is done by following the instructions from Poole et al. (2008). A source region is chosen as a circular region of 5 arcsecs centered at the source location, while the background region is selected away from the source location with an area 3 times larger than the source region. The observed flux was corrected for galactic extinction by using $E(V-B) = 0.017$ and $R_V = A_V/E - B = 3.1$, following (Schlegel et al., 1998; Schlafly and Finkbeiner, 2011).

2.3. Fermi-LAT

The *Fermi* Large Area Telescope (LAT) is a space-based high energy telescope with a wide field of view $\sim 2.4 \text{ Sr}$ (Atwood et al., 2009). It is part of the *Fermi* γ -ray space Telescope, launched by NASA in 2008. *Fermi*-LAT operates primarily in scanning mode, monitoring the entire sky in the energy range of approximately 20 MeV to 500 GeV every three hours. We acquired the *Fermi*-LAT γ -ray data of Mrk 501 during the time period MJD 57615.2 – 59666. The data was processed using Fermitools version 2.2.0, following standard analysis procedures outlined in *Fermi*-LAT documentation (Wood et al., 2017). Photon events with a high

¹http://www.tifr.res.in/~astrosat_sxt/dataanalysis.html

probability were extracted specifically within a $15'$ region of Interest (ROI) centered at the source location. The analysis was conducted within the energy range of $0.1 - 300$ GeV, employing the P8R3_SOURCE_V3 instrument response function (IRF) with specified parameters `evclass=128` and `evtype=3`. XML files were generated utilizing the galactic diffusion model `gll_iem_v07.fits` and the isotropic background model `iso_P8R3_SOURCE_V3_v1.txt`. Additionally, spectral models and parameters for sources within the ROI were obtained from the fourth *Fermi* source catalog. Subsequently, flux points and corresponding energies from *Fermi*-LAT observations were converted to a format compatible with XSPEC (PHA format) using the `ftflx2xsp` tool.

3. AstroSat Results

3.1. Temporal Analysis

To explore the X-ray variability of Mrk 501, we utilized simultaneous observations of SXT and LAXPC instruments onboard *AstroSat* during the period MJD 57615 – 59666. Mrk 501 were observed five times during the integration period, with observation details provided in Table 1. We obtained 100-second binned SXT and LAXPC light curve for each observation (see Figure 1). The resulting light curves were analyzed using the LCSTATS tool, leading to the determination of RMS fractional variation values, which are mentioned in Table 2. The obtained RMS fractional values indicate subtle variability in the source. Moreover, the maximum count rate acquired in all the observations (see Table 2) suggests that the source remained mostly in a low flux state. These observations provide an opportunity to investigate Mrk 501 during its low flux states, facilitating an enhanced understanding of the underlying emission processes.

3.2. Spectral Analysis

In order to understand the X-ray spectral behavior of Mrk 501, we conducted a joint spectral fitting of SXT and LAXPC spectra obtained in the energy range $0.3 - 6.0$ keV and $3.0 - 30.0$ keV, respectively, for all the five selected observations. Further, to account for the absorption due to neutral hydrogen, we used the galactic column density value as $n_H = 1.69 \times 10^{20} cm^{-2}$ (Kalberla et al., 2005).

Three distinct models, namely the power-law (PL), broken power-law (BPL), and logparabola (LP) models, were employed to fit the spectrum. The PL model is defined as

$$n(E) = K \cdot E^{-\Gamma}, \quad (1)$$

where K is normalization at 1 keV, and Γ is the photon index. The LP model is defined as

$$n(E) = K(E/E_{pivot})^{-(\alpha+\beta \log(E/E_{pivot}))} \quad (2)$$

where α is the photon-index at pivot energy $E_{pivot} = 1$ keV, β is the curvature parameter, and K is the normalization. The BPL model is defined as

$$n(E) = \begin{cases} KE^{-\Gamma_1} & \text{for } E < E_b \\ KE_b^{\Gamma_2-\Gamma_1} E^{-\Gamma_2} & \text{for } E \geq E_b \end{cases} \quad (3)$$

where K is normalization, E_b is break energy, Γ_1 and Γ_2 indicate the photon indices before and after break energy E_b . The combined broad X-ray spectra were fitted with the $constant \times tbabs \times PL/BPL/LP$ model. The constant was considered to take into account any systematic difference in the effective areas of LAXPC and SXT. The best-fit parameters of these models for the five observations are given in Table 3. As shown in the table, the PL model results in highly reduced- χ^2 values compared to the BPL and LP models. The combined SXT and LAXPC X-rays spectra fitted with BPL and LP models are shown in Figure 3. In the case of BPL, the spectral indices before and after break energy are obtained in the range $1.84 - 2.21$ and $2.30 - 2.76$, respectively with break energy between $2.32 - 3.33$ keV. During the hard spectrum, the source is brighter as compared to other observations. In the LP model, the spectral indices denoted as α ranged between $1.66 - 2.20$ and β values $0.18 - 0.36$. These values indicate that the spectra of the source exhibit slight to moderate curvature. Notably, the parameters of the LP model are consistent with those of the BPL model, with the α parameter of the LP model being the hardest for the same observation where BPL indices are hardest. Additionally, for the hardest spectrum observation, the curvature parameter shows a maximum value of 0.36. The variation of α with the mean count rate shown in Figure 2 suggest harder when brighter feature in the source. Similarly, the variations of the spectral indices obtained from the BPL (lower energy index) and PL models with the mean count rates exhibit the same trend, as depicted in the Figure 2.

4. Multi-wavelength Analysis

4.1. Multi-wavelength light curve (MWLC)

In addition to the *AstroSat* LAXPC and SXT data, we utilized *Swift*-UVOT and *Fermi*-LAT data observed during the MJD 57615 – 59666 to explore the temporal and spectral behavior of source across a broad range of energies. The MWLC obtained using the observations from *Swift*-UVOT, *AstroSat*-SXT/LAXPC20, and *Fermi*-LAT is shown in Figure 4. *AstroSat* conducted five observations of Mrk 501 during MJD 57600 – 59665, but due to limited simultaneous UVIT observations in the *AstroBrowse*, we relied on *Swift*-UVOT observations. The MWLC shows that the source has remained mostly in the low flux states. Notably, the MAGIC Collaboration has also reported a historically low flux state in the source during the period 2017 – 2019 (Abe et al., 2023). Therefore, *AstroSat* observations together with *Fermi*-LAT and *Swift*-UVOT data provide an opportunity to carry out a detailed broadband study of the Mrk 501 in the low flux state.

4.2. Fractional Variability

To assess the variability of the source in the low flux state, we computed the fractional variability of the light curves across different energy bands. We employed the procedure outlined in the (Vaughan et al., 2003), wherein the fractional variability F_{var} is determined using the formula

Table 1: *AstroSat/Swift-UVOT* observation details of Mrk 501. Column 1: Observation, 2: Observation ID, 3: Instrument, 4: Date (MJD), 5: Mode of receiving data, 6: Exposure time.

Observation (1)	Observation ID (2)	Instrument (3)	Date(MJD) (4)	Mode (5)	Exposure Time(ks) (6)
S1	G05 218T05 9000000602 00092398007	<i>AstroSat</i> <i>Swift-UVOT</i>	(57615.2 – 57615.9) (57614.2)	PC PC	29.7 0.96
S2	A05 107T01 9000002852 00095331002	<i>AstroSat</i> <i>Swift-UVOT</i>	(58594.9 – 58596.2) (58594.0)	PC PC	30 0.81
S3	A07 101T02 9000003544 00095341008	<i>AstroSat</i> <i>Swift-UVOT</i>	(58910.3 – 58912) (58914.8)	PC PC	34.3 0.87
S4	A07 145T01 90000003594 00095341012	<i>AstroSat</i> <i>Swift-UVOT</i>	(58934.5 – 58939.8) (58942.3)	PC PC	106 0.51
S5	T05 015T01 9000005026 00096029018 00011184185 00011184186 00011184187	<i>AstroSat</i> <i>Swift-UVOT</i> <i>Swift-UVOT</i> <i>Swift-UVOT</i> <i>Swift-UVOT</i>	(59662.3 – 59665.8) (59662.3) (59663.10) (59664.1) (59665.1)	PC PC PC PC PC	82.8 1.03 0.81 1.07 1.06

Table 2: Details of the LCSTATS analysis done on the SXT (0.3 – 7.0 keV) and LAXPC (3.0 – 30.0 keV) light curves. Columns 1: Observation, 2: Instrument, 3: Counts/sec, 4: RMS fractional variability.

Observation	Instrument	(Counts/sec)	F_{var}
S1	SXT	2.68 ± 0.16	0.06 ± 0.007
	LAXPC	8.61 ± 0.90	0.07 ± 0.02
S2	SXT	1.76 ± 0.13	0.07 ± 0.01
	LAXPC	6.09 ± 0.91	0.08 ± 0.04
S3	SXT	1.89 ± 0.18	0.03 ± 0.08
	LAXPC	7.90 ± 0.90	0.04 ± 0.07
S4	SXT	2.92 ± 0.42	0.08 ± 0.003
	LAXPC	13.51 ± 0.98	0.09 ± 0.005
S5	SXT	5.16 ± 0.87	0.03 ± 0.006
	LAXPC	21.46 ± 0.91	0.04 ± 0.003

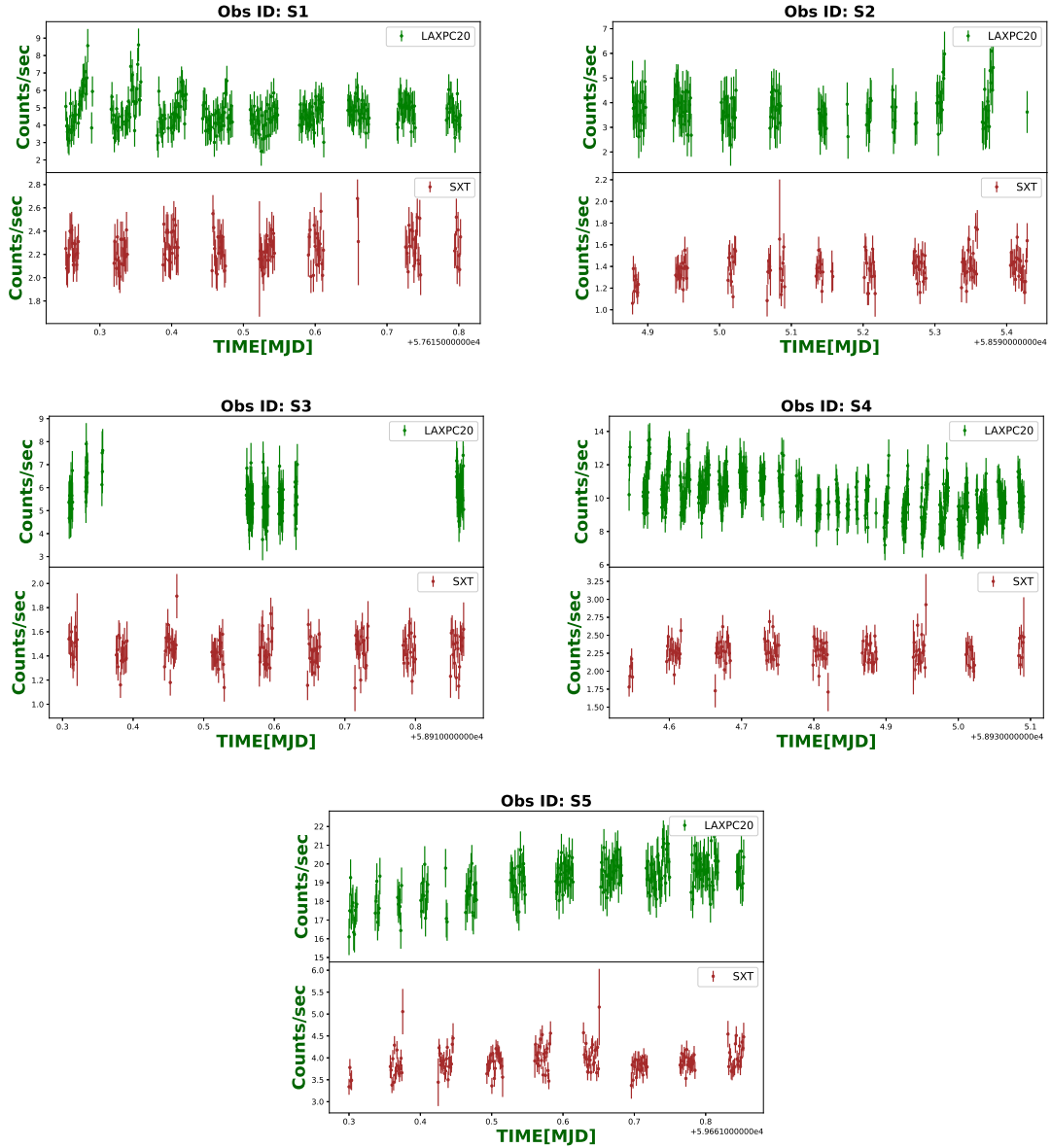


Figure 1: Simultaneous 100 second binned SXT (0.3 – 7.0 keV) and LAXPC (3.0 – 30.0 keV) light curves of Mrk 501. Top left S1 observation, top right S2 observation, middle left S3 observation, middle right S4 observation, and bottom S5 observation.

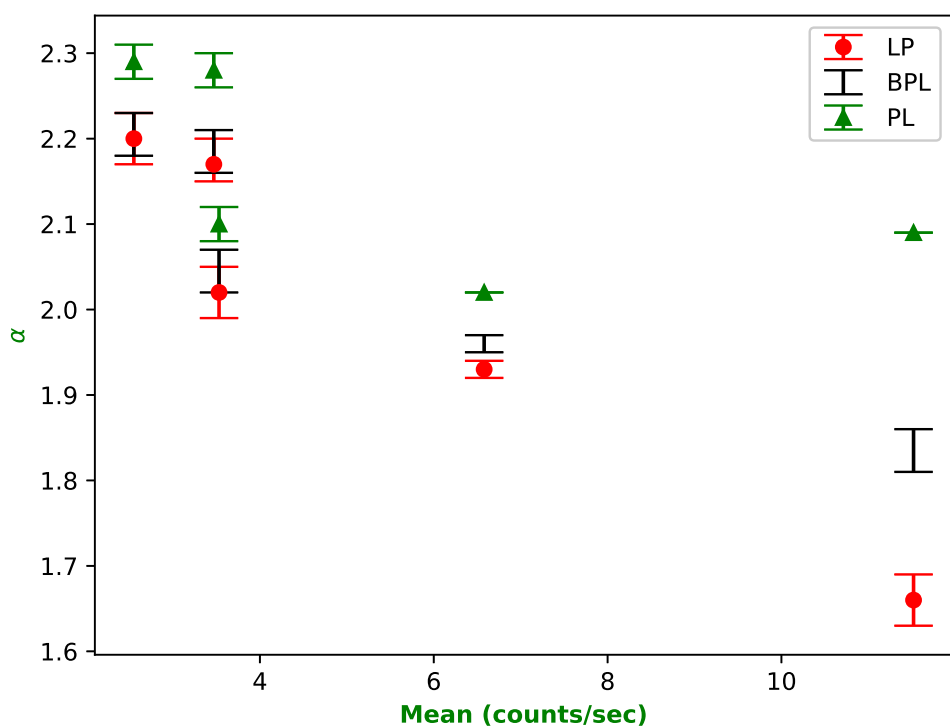


Figure 2: Spectral index versus the mean count rates obtained by fitting the joint SXT-LAXPC spectrum with the LP, BPL and PL models.

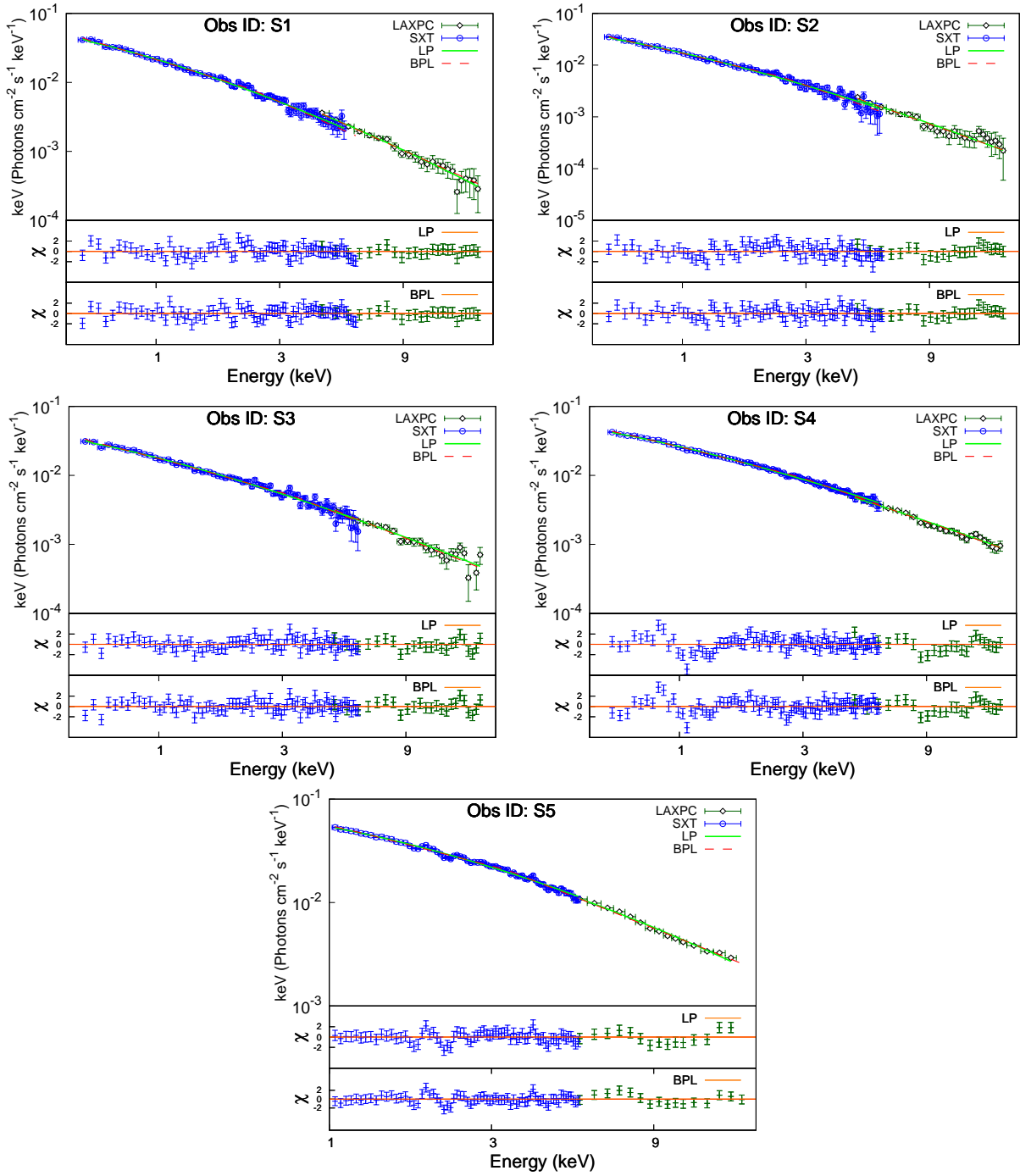


Figure 3: The combined SXT and LAXPC spectrum fitted with the constant*TBabs*LP/BPL model. The five plots correspond to S1 (top left), S2 (top right), S3 (middle left), S4 (middle right), and S5 (bottom) observations.

Table 3: The best-fit parameters obtained by fitting the combined SXT and LAXPC spectrum with the constant*tbabs*BPL/LP/PL models. Columns 1: Observation 2: Model 3: Index before break energy / PL index 4: Index after break energy 5: Index at pivot energy 6: Curvature parameter 7: Norm 8: Constant factor and 9: Reduced- χ^2

Observation	Model	Γ_1	break energy	Γ_2	α	β	norm	factor	χ^2_{red}
S1	BPL	$2.19^{+0.02}_{-0.02}$	$2.32^{+0.49}_{-0.19}$	$2.67^{+0.02}_{-0.02}$			$0.02^{+0.002}_{-0.002}$	$0.80^{+0.06}_{-0.06}$	90.62/98=0.92
	LP				$2.17^{+0.02}_{-0.03}$	$0.29^{+0.05}_{-0.05}$	$0.02^{+0.001}_{-0.001}$	$0.86^{+0.06}_{-0.05}$	98.35/99=0.99
	PL	$2.28^{+0.02}_{-0.02}$					$0.02^{+0.002}_{-0.001}$	$1.13^{+0.06}_{-0.05}$	183.64/100=1.83
S2	BPL	$2.21^{+0.02}_{-0.02}$	$2.42^{+0.45}_{-0.33}$	$2.76^{+0.10}_{-0.09}$			$0.01^{+0.002}_{-0.002}$	$0.80^{+0.09}_{-0.08}$	99.24/99=0.98
	LP				$2.20^{+0.03}_{-0.03}$	$0.28^{+0.06}_{-0.06}$	$0.01^{+0.001}_{-0.001}$	$0.91^{+0.08}_{-0.07}$	119.78/99=0.97
	PL	$2.29^{+0.02}_{-0.02}$					$0.01^{+0.002}_{-0.001}$	$1.23^{+0.08}_{-0.07}$	176.69/100=1.76
S3	BPL	$2.05^{+0.02}_{-0.02}$	$3.24^{+0.45}_{-0.33}$	$2.46^{+0.10}_{-0.09}$			$0.01^{+0.001}_{-0.001}$	$0.93^{+0.07}_{-0.07}$	99.24/99=1.00
	LP				$2.02^{+0.03}_{-0.03}$	$0.20^{+0.05}_{-0.05}$	$0.02^{+0.001}_{-0.001}$	$1.01^{+0.29}_{-0.46}$	97.14/100=0.97
	PL	$2.10^{+0.02}_{-0.02}$					$0.01^{+0.002}_{-0.001}$	$1.22^{+0.06}_{-0.06}$	132.14/101=1.30
S4	BPL	$1.96^{+0.01}_{-0.01}$	$2.90^{+0.27}_{-0.21}$	$2.30^{+0.02}_{-0.02}$			$0.02^{+0.001}_{-0.001}$	$1.02^{+0.04}_{-0.04}$	148.26/107=1.38
	LP				$1.93^{+0.01}_{-0.01}$	$0.18^{+0.02}_{-0.02}$	$0.02^{+0.001}_{-0.001}$	$1.09^{+0.03}_{-0.04}$	169.55/108=1.56
	PL	2.02^-_-					0.02^-_-	1.30^-_-	316.82/109=2.90
S5	BPL	$1.84^{+0.02}_{-0.02}$	$3.33^{+0.26}_{-0.20}$	$2.31^{+0.02}_{-0.02}$			$0.05^{+0.001}_{-0.001}$	$1.0^{+0.04}_{-0.04}$	67.25/83=0.81
	LP				$1.66^{+0.03}_{-0.03}$	$0.36^{+0.04}_{-0.04}$	$0.05^{+0.002}_{-0.002}$	$1.03^{+0.02}_{-0.02}$	76.06/83=0.91
	PL	2.09^-_-					0.06^-_-	1.0^-_-	486.67/86=5.65

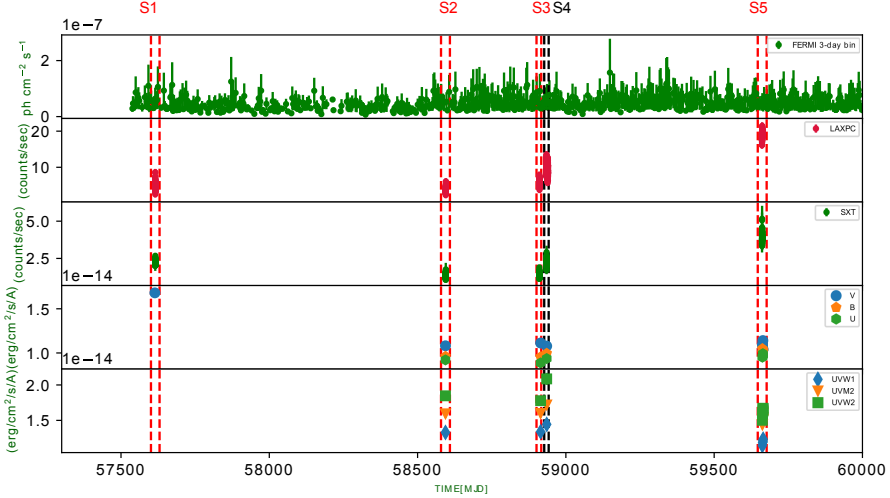


Figure 4: Multi-wavelength light curve (MWLC) obtained from *AstroSat* (SXT, LAXPC), *Swift*-UVOT, and *Fermi*-LAT observations. The 3-day bin γ -ray light curve, acquired in the energy range of 0.3–300 GeV, is shown in the top panel. The 100-second binned SXT and LAXPC light curves, which were produced by integrating photons in the energy ranges of 0.3 and 7.0 keV and 3.0 and 30.0 keV, respectively, are displayed in the second and third panels. The optical/UV light curves are shown in final two panels, each point corresponds to individual observation ID. S1, S2, S3, S4 and S5 states represented by dashed vertical lines indicate the time intervals for which broadband spectral modeling is performed.

$$F_{var} = \sqrt{\frac{S^2 - \overline{\sigma_{err}^2}}{\overline{F}^2}} \quad (4)$$

where S^2 is the variance, \overline{F} is the mean, and $\overline{\sigma_{err}^2}$ is the mean square of the measurement error on the flux points. The uncertainty on F_{var} is given by Vaughan et al. (2003)

$$F_{var,err} = \sqrt{\frac{1}{2N} \left(\frac{\overline{\sigma_{err}^2}}{F_{var}\overline{F}^2} \right)^2 + \frac{1}{N} \frac{\overline{\sigma_{err}^2}}{\overline{F}^2}} \quad (5)$$

Here, N represents the number of flux points in the light curve.

The values of F_{var} along with the uncertainties obtained for γ -ray, X-ray, and Optical/UV light curves are shown in Table 4, and the plot between F_{var} and energy is shown in Figure 5. Notably, the X-ray band exhibits a large variability amplitude value compared to the values obtained in Optical/UV and γ -ray bands. This variability pattern resembles the characteristic double hump feature observed in the broadband SED of Mrk 501. The X-ray spectra, lying around the SED peak, are primarily attributed to high-energy electrons, whereas the γ -ray and optical spectra, positioned before the break energy, arise from low-energy electrons. The faster cooling of high-energy electrons emitting X-rays may lead to a larger variability amplitude at the X-ray band, while the slower cooling of low-energy electrons may result in a smaller variability amplitude at the Optical/UV and γ -ray band.

5. Broadband spectral analysis

These simultaneous observation offers an opportunity to model the emission of the source with enhanced reliability in

the low flux states. Notably, previous modeling efforts were mainly based on the high activity state of Mrk 501. Although the source was previously examined during its low activity state, the simultaneous observations used for modeling were limited (Anderhub et al., 2009).

We modeled the broadband SED of Mrk 501 by considering a one-zone leptonic model involving synchrotron and SSC processes. In the model, we assume that emission originates from a spherical region of radius R filled with a relativistic particle distribution $n(\gamma)$. The emission region moves down the jet with bulk Lorentz factor Γ at a small angle θ with respect line of sight of an observer. The close pointing of the relativistic jet results in the Doppler-boosted emission, which is taken into account by incorporating the Doppler factor, $\delta = \frac{1}{\Gamma(1-\beta \cos\theta)}$. The relativistic particles in the emission region undergo synchrotron and IC losses in the presence of magnetic fields and seed photons, respectively. In our model, we assume the SSC process, so seed photons for IC process are synchrotron photons from the jet itself. The electron Lorentz factor, γ is expressed in terms of new variable ξ , such that $\xi = \gamma \sqrt{C}$, where $C = 1.36 \times 10^{-11} \frac{\delta B}{1+z}$ with z being the redshift of source. The synchrotron flux received by the observer with ξ as parameter can be written as (Shah, 2023)

$$F_{syn}(\epsilon) = \frac{\delta^3(1+z)}{d_L^2} V \mathbb{A} \int_{\xi_{min}}^{\xi_{max}} f(\epsilon/\xi^2) n(\xi) d\xi, \quad (6)$$

where d_L is luminosity distance, V is the volume of emission region, $\mathbb{A} = \frac{\sqrt{3}\pi e^3 B}{16m_e c^2 \sqrt{C}}$, ξ_{min} and ξ_{max} correspond to the minimum and maximum energy of electron, and $f(x)$ is the synchrotron emissivity function (Rybicki and Lightman, 1986). The SSC flux received by the observer at energy ϵ can be obtained using

Table 4: Fractional variability amplitude F_{var} obtained in different energy bands. Columns 1: energy band 2: fractional variability amplitude.

Energy band	F_{var}
γ -ray (0.1 – 300 GeV)	0.35 ± 0.08
LAXPC (3.0 – 30.0 keV)	0.46 ± 0.003
SXT (0.3 – 7.0 keV)	0.41 ± 0.002
UVW2	0.09 ± 0.05
UVM2	0.04 ± 0.01
UVW1	0.07 ± 0.02
U	0.02 ± 0.01
B	0.02 ± 0.01
V	0.18 ± 0.01

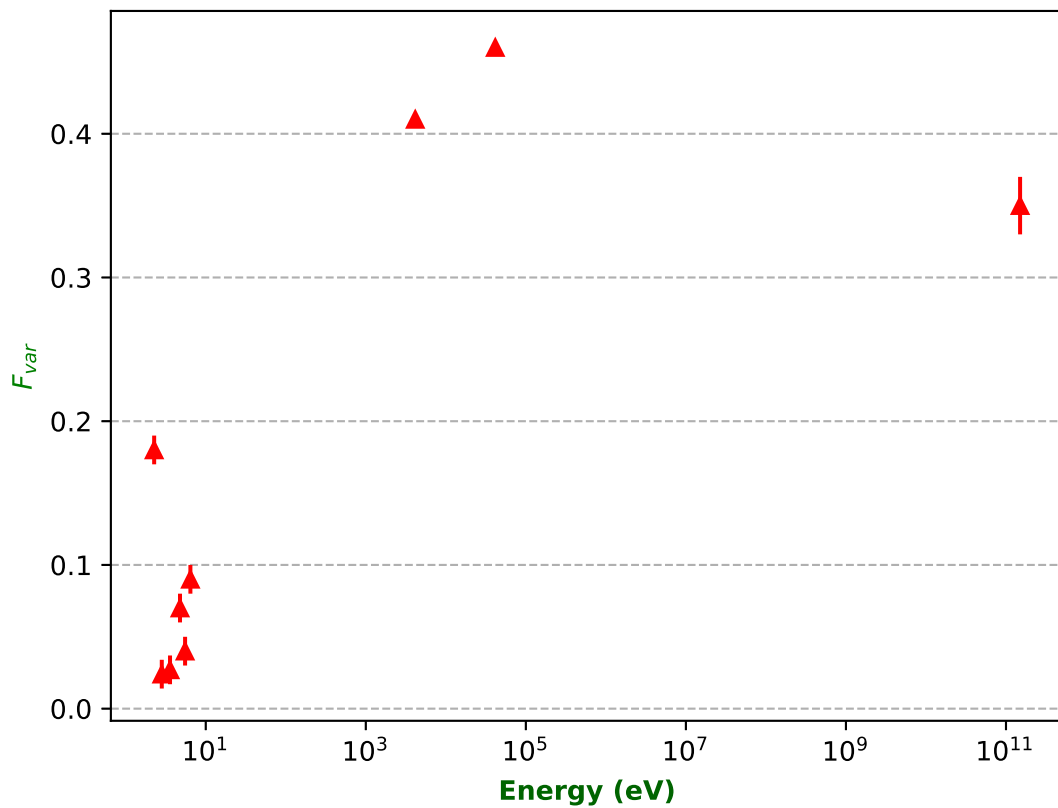


Figure 5: Fractional variability amplitude obtained in different energy bands is plotted against the energy.

the equation

$$F_{ssc}(\epsilon) = \frac{\delta^3(1+z)}{d_L^2} V \mathbb{B} \epsilon \int_{\xi_{min}}^{\xi_{max}} \frac{1}{\xi^2} \int_{x_1}^{x_2} \frac{I_{syn}(\epsilon_i)}{\epsilon_i^2} f(\epsilon_i, \epsilon, \xi / \sqrt{C}) d\epsilon_i n(\xi) d\xi \quad (7)$$

where, ϵ_i is incident photon energy, $\mathbb{B} = \frac{3}{4} \sigma_T \sqrt{C}$, $I_{syn}(\epsilon_i)$ is the synchrotron intensity, $x_1 = \frac{C\epsilon}{4\xi^2(1-\sqrt{C}\epsilon/\xi m_e c^2)}$, $x_2 = \frac{\epsilon}{(1-\sqrt{C}\epsilon/\xi m_e c^2)}$ and

$$f(\epsilon_i, \epsilon, \xi) = 2q \log q + (1+2q)(1-q) + \frac{\kappa^2 q^2 (1-q)}{2(1+\kappa q)}$$

here $q = \frac{C\epsilon}{4\xi^2 \epsilon_i (1-\sqrt{C}\epsilon/\xi m_e c^2)}$ and $\kappa = \frac{4\xi \epsilon_i}{\sqrt{C} m_e c^2}$.

The Equations 6 and 7 are solved numerically and the resultant numerical code is incorporated as a local convolution model in XSPEC. In the convolved XSPEC model ‘energy’ variable is interpreted as $\xi = \gamma \sqrt{C}$. The convolution model enables the statistical fitting of broadband SED and allows us to model the broadband spectrum for any particle energy distribution $n(\xi)$. In our work, we considered different forms of $n(\xi)$ like BPL, LP, energy-dependent acceleration (EDA) model, and particle distribution with maximum energy (ξ_{max}) model to fit the broadband SED. Aforementioned, particle distributions like LP and BPL are defined in equations 2 and 3, respectively. For the ξ_{max} model, we considered the scenario in which shock-induced particle acceleration leads to radiative energy loss. Given that the radiative loss is proportional to the square of energy, the loss becomes more significant at higher energies, consequently shaping the particle distribution with maximum energy. The form of particle energy distribution can be written as (after transforming γ to $\xi = \sqrt{C}\gamma$) (Hota et al., 2021)

$$n(\xi) = K \xi^{-p} \left(1 - \frac{\xi}{\xi_{max}}\right)^{(p-2)} \quad (8)$$

where K is particle normalization, p is the particle spectral index and $\xi_{max} = \gamma_{max} \sqrt{C}$ is Lorentz factor corresponding to maximum particle energy.

We have also taken into consideration a scenario in which the acceleration process is energy dependent through the relation $\tau_{acc} = \tau_{acc,R} \left(\frac{\gamma}{\gamma_R}\right)^\kappa$, where τ_{acc} is the acceleration time scale, γ_R is the Lorentz factor corresponding to a gyration radius that matches with the size emission region. The situation can be visualized by assuming that the electrons gain relativistic energy by crossing a shock front and this acceleration ceases when they diffuse away from the shock. The particle distribution for this case can be obtained as (Hota et al., 2021)

$$n(\xi) = K \xi^{\kappa-1} \exp\left[-\frac{\psi}{\kappa} \xi^\kappa\right] \quad (9)$$

where K is normalization, ψ is parameter which depends on τ_{esc} and κ through relation $\psi = \tau_{acc,R}/\tau_{esc} (C\gamma_R^2)^{-\kappa/2}$.

Using the convolved SED model involving synchrotron and SSC processes, the observed broadband spectrum is determined

mainly by parameters such as N , Γ , B , R , θ , ξ_{min} , ξ_{max} and alongside parameters related to the underlying particle distribution. For example, if the underlying particle distribution is EDA model, the additional parameters include κ and ψ . The convolution broadband SED code also enables the fitting of the SED with jet power P_{jet} as one of the parameters; however, in this scenario, N must remain a fixed parameter.

By adopting the conventional method, which assumes the inertia of the jet is mainly contributed by cold protons, equal in number to non-thermal electrons, we estimated the total jet power as (Celotti and Ghisellini, 2008; Ghisellini et al., 2014)

$$P_{jet} = \pi R^2 \Gamma^2 \beta c (U_e + U_p + U_B) \quad (10)$$

where Γ is the bulk Lorentz factor of the jet, $\beta = \frac{v}{c}$ is the velocity of the jet in units of the speed of light, R is the radius of the jet, U_e , U_p , and U_B are the energy density of the electrons, protons, and the magnetic field respectively.

The limited amount of information from Optical/UV, X-ray, and γ -ray makes it difficult to constrain the full set of parameters. Consequently, we performed the broadband fitting by allowing the parameters Γ , B , α , β , and Norm/P_{jet} to vary when the particle distribution follows a logparabola model. In the case of a broken power-law model, the parameters Γ , B , particle indices before and after break energy (Γ_1 and Γ_2), and Norm/P_{jet} were varied. For the EDA model, the parameters Γ , B , κ , ψ , and Norm/P_{jet} were adjusted, and for the γ -max model, the parameters Γ , B , p , ξ_{max} , and Norm/P_{jet} were varied. Other parameters for these models were fixed to typical values necessary for the observed broadband spectrum. For example, we have frozen the parameters R , Γ , and θ at 10^{17} cm, 20, and 2 degree respectively in all the observations. These values are comparable with those used in previous studies conducted on the non-flaring emission of the source (Abdo et al., 2011; Anderhub et al., 2009). Additionally, to achieve a reasonable reduced- χ^2 in all the observations, we added a systematic error of 3% to the X-ray and γ -ray data and 20% to the Optical/UV data. We noted that the broadband SED fit with the four considered particle distributions yielded similar reduced- χ^2 values for all observations. The reduced- χ^2 values imply a degeneracy in the underlying particle distributions. The best-fit parameter values along with the reduced- χ^2 for five observations are summarised in Table 5 and the broadband SED points along with model fits are shown in Figure 6.

5.1. Correlation analysis

The four models for the particle distribution yielded similar reduced- χ^2 values, indicating a degeneracy in the underlying particle distributions. However, the best-fit parameters and properties acquired from these models can be used to remove the degeneracy and rule out some of the models. Specifically, the jet power estimated from the ξ_{max} model shows significantly higher values in all the observations compared to those obtained using other forms of particle distribution. Consequently, based on the criterion of minimum jet power, we can exclude the ξ_{max} model as a plausible form of particle distribution. Additionally, the LP model being an approximation of the EDA model

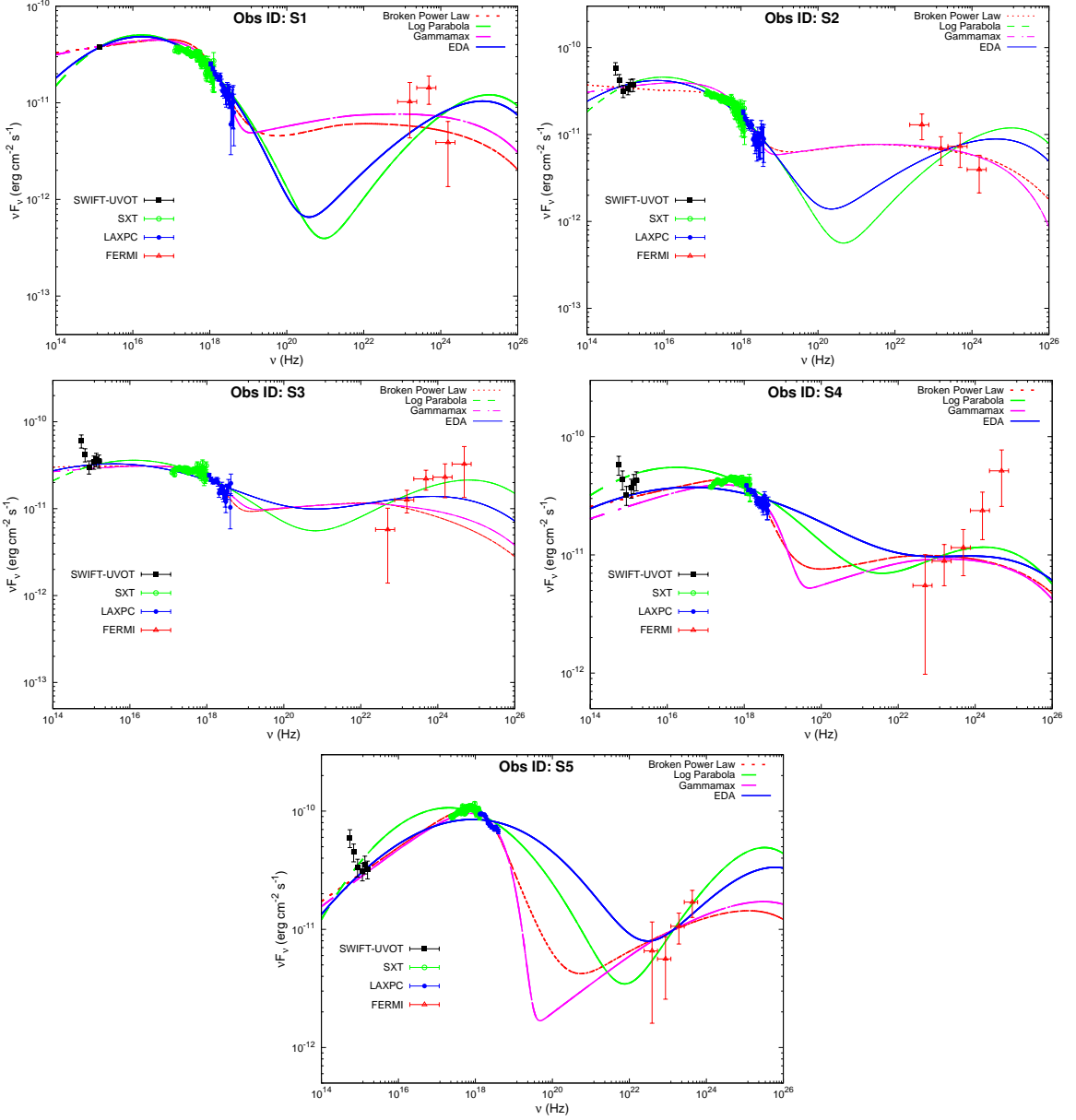


Figure 6: Broadband SED plots are generated for each observation using four distinct particle distribution models: LP, BPL, EDA, and ξ_{max} . The top-left plot corresponds to observation (S1), the top-right plot to observation (S2), the middle-left plot to observation (S3), the middle-right plot to observation (S4), and the bottom plot to observation (S5).

Table 5: Details of the best t parameters obtained by fitting the broadband spectrum of Mrk 501 with the one zone SED added as a local model in XSPEC. In the table, Columns 1: Observations, 2: Particle distribution models 3: Bulk Lorentz factor, 4, 5, 6: represents the parameters corresponding to chosen particle distribution, 7: Magnetic field in units of Gauss, 8: Jet power in logarithmic scale in units of erg sec⁻¹, 9: Reduced- χ^2 . The subscript and superscript on the parameter values denote the lower and upper bound errors respectively, while – indicates the lower or upper bound error is not constrained.

Observation (1)	Model (2)	Γ (3)	(4)	(5)	(6)	B(G) (7)	P_{jet} (8)	χ^2_{red} (9)
S1	LP	20	$\alpha^{+0.05}_{-0.04}$	$\beta^{+0.08}_{-0.05}$		$0.003^{+0.0008}_{-0.0007}$	$43.85^{+0.16}_{-0.25}$	0.96
	BPL	20	$\Gamma_1^{+0.05}_{-0.04}$	$E_{break}^{+0.2}_{-0.1}$	$\Gamma_2^{+0.32}_{-0.30}$	$0.01^{+0.008}_{-0.005}$	$46.49^{+0.16}_{-0.23}$	0.73
	EDA	20	$\kappa^{+0.07}_{-0.01}$	$\psi^{+0.03}_{-0.03}$		$0.005^{+0.001}_{-0.0007}$	$44.41^{+0.21}_{-0.28}$	0.86
	ξ_{max}	20	$p^{+0.02}_{-0.01}$	$\xi_{max}^{+0.21}_{-0.20}$		$0.01^{+0.002}_{-0.001}$	$53.67^{+0.21}_{-0.31}$	0.72
S2	LP	20	$\alpha^{+0.02}_{-0.02}$	$\beta^{+0.005}_{-0.006}$		$0.006^{+0.0005}_{-0.0004}$	$44.00^{+0.12}_{-0.19}$	1.34
	BPL	20	$\Gamma_1^{+0.03}_{-0.05}$	$E_{break}^{+0.3}_{-0.1}$	$\Gamma_2^{+2.54}_{-1.35}$	$0.01^{+0.002}_{-0.009}$	$46.71^{+0.11}_{-0.17}$	0.96
	EDA	20	$\kappa^{+0.003}_{-0.003}$	$\psi^{+0.04}_{-0.04}$	–	$0.002^{+0.003}_{-0.0005}$	$44.81^{+0.27}_{-0.35}$	1.26
	ξ_{max}	20	$p^{+0.01}_{-0.09}$	$\xi_{max}^{+0.28}_{-0.56}$		$0.01^{+0.002}_{-0.001}$	$54.03^{+0.28}_{-0.56}$	1.08
S3	LP	20	$\alpha^{+0.01}_{-0.02}$	$\beta^{+0.04}_{-0.04}$		$0.005^{+0.002}_{-0.009}$	$45.10^{+0.16}_{-0.19}$	1.43
	BPL	20	$\Gamma_1^{+0.02}_{-0.01}$	$E_{break}^{+0.1}_{-0.2}$	$\Gamma_2^{+0.87}_{-0.77}$	$0.01^{+0.002}_{-0.001}$	$46.90^{+0.14}_{-0.14}$	1.11
	EDA	20	$\kappa^{+0.004}_{-0.005}$	$\psi^{+0.03}_{-0.03}$		$0.007^{+0.001}_{-0.009}$	$46.00^{+0.14}_{-0.30}$	1.33
	ξ_{max}	20	$p^{+0.01}_{-0.09}$	$\xi_{max}^{+0.16}_{-0.16}$		$0.007^{+0.002}_{-0.0009}$	$54.37^{+0.16}_{-0.40}$	1.18
S4	LP	20	$\alpha^{+0.03}_{-0.02}$	$\beta^{+0.01}_{-0.006}$		$0.03^{+0.008}_{-0.008}$	$43.57^{+0.14}_{-0.19}$	1.06
	BPL	20	$\Gamma_1^{+0.02}_{-0.01}$	$E_{break}^{+0.02}_{-0.01}$	$\Gamma_2^{+1.20}_{-0.83}$	$0.01^{+0.001}_{-0.001}$	$46.50^{+0.10}_{-0.07}$	0.94
	EDA	20	$\kappa^{+0.002}_{-0.004}$	$\psi^{+0.02}_{-0.02}$		$0.005^{+0.005}_{-0.001}$	$45.43^{+0.25}_{-0.48}$	1.36
	ξ_{max}	20	$p^{+0.01}_{-0.01}$	$\xi_{max}^{+0.61}_{-0.55}$		$0.006^{+0.002}_{-0.001}$	$53.42^{+0.61}_{-0.20}$	1.04
S5	LP	20	$\alpha^{+0.02}_{-0.04}$	$\beta^{+0.02}_{-0.009}$		$0.01^{+0.002}_{-0.001}$	$43.56^{+0.02}_{-0.05}$	0.75
	BPL	20	$\Gamma_1^{+0.01}_{-0.02}$	$E_{break}^{+0.03}_{-0.02}$	$\Gamma_2^{+1.1}_{-0.74}$	$0.03^{+0.001}_{-0.001}$	$45.67^{+0.12}_{-0.17}$	1.42
	EDA	20	$\kappa^{+0.002}_{-0.004}$	$\psi^{+0.02}_{-0.02}$		$0.005^{+0.001}_{+0.004}$	$44.82^{+0.12}_{-0.22}$	1.20
	ξ_{max}	20	$p^{+0.02}_{-0.01}$	$\xi_{max}^{+0.51}_{-0.44}$		$0.009^{+0.001}_{-0.002}$	$52.60^{+0.42}_{-0.42}$	1.45

(Hota et al., 2021), implies that the underlying mechanism responsible for the particle distribution is the same in both models. Therefore, it is equivalent to consider either of the models. Due to the simpler form of the LP, we opted for this model and the BPL model for subsequent analysis. To further constrain the particle distribution and accurately estimate the P_{jet} in different observations of Mrk 501, we conducted a comprehensive correlation analysis of the P_{jet} with the Γ , γ_{min} and R (see Figure 7 and 8). In the correlation plots, we calculated P_{jet} for different values of Γ , γ_{min} and R . We also explored the correlation of R with the magnetic field (right bottom panel of Figures 7 and 8), here magnetic field is estimated for different values of R . Notably, we observed that the P_{jet} consistently increased with a rise in Γ for both models. Next, we fixed $\Gamma \sim 20$ and calculated the P_{jet} for different values of minimum particle energy. In the LP model, we found that the P_{jet} is independent of γ_{min} . While in the BPL model, the P_{jet} exhibited a decrease trend with an increase in γ_{min} . We further investigated the impact of varying the size (R) on the P_{jet} . In the LP model, P_{jet} increased with a rise in R , whereas in the BPL model, P_{jet} remained constant for different R values. Additionally, our analysis revealed that, in both models, the size of the emission region required decreased with an increase in the magnetic field.

6. Summary and Discussion

The BL Lac object, Mrk 501, has been observed by the *Fermi*-LAT instrument since its launch. For the first time, these observations together with the simultaneous observations of *AstroSat* and *Swift*-UVOT have enabled a comprehensive temporal and spectral study of the source. Our analysis of the 3-day binned γ -ray light curve revealed that the emission during this period MJD 57615 – 59666 corresponded to a quiescent state of the source. These results made Mrk 501 an important blazar source to understand the underlying physics. Since in most blazars, the multifrequency data is available in high flux states, and very sparse data is available in low flux states. This is primarily because multifrequency campaigns are triggered by observing enhanced flux levels in some energy bands. Hence much of our understanding of the blazars is biased towards high-activity states, where perhaps distinct physical processes play a dominant role. Hence, it is important to study the source in the low flux states. In the case of Mrk 501, the long-duration observations are available in the low flux state from multiple Telescopes. In the X-ray range, *AstroSat* has archived five observations during the period MJD 57615 – 59666. These observations suggest that Mrk 501 was predominantly in a low flux state, though the flux (counts/second) exhibited a slight increase during the period MJD 58910.3 – 59665.8. A recent study conducted by (Abe et al., 2023) has also indicated a historically low flux for Mrk 501 from mid-2017 to mid-2019. The long-lasting stable emission can potentially be explained by a standing shock scenario proposed by (Marscher et al., 2008) and further explored in (Marscher et al., 2014). Our analysis of the temporal behavior of Mrk 501 using SXT and LAXPC light curves showed notable variability during the source's low flux state. A comparison of variability across different energy

bands indicated that the maximum variability occurred in the X-ray band as compared to the optical and γ -ray band. These findings are consistent with previous studies conducted during both low and high flux states. Schleicher et al. (2019) analyzed data from different instruments, including FACT, Swift XRT/BAT, and Fermi telescopes, over the period from January 2013 to June 2018. The study observed that variability is significantly larger in X-rays compared to γ -rays in both Mrk 501 and Mrk 421. Additionally, in the VHE regime, the variability was found to be more pronounced in Mrk 501 than in Mrk 421. During the 2008 campaign on Mrk 501, it was observed that variability was greater in X-rays and VHE compared to optical wavelengths (Aleksić et al., 2015). More recent studies by Abe et al. (2023); Kapanadze et al. (2023) examined the source during a low flux state. Similarly, they found that X-ray variability is larger than that observed in γ -ray and optical data. These findings are consistent with our studies and further validate our conclusions on the significant variability observed in X-rays across different flux states. In Mrk 501, the amplitude of variability in distinct energy bands corresponds to the shape of the broadband SED. Given that the X-ray spectrum in the broadband SED lies around the peak, it is therefore mostly associated with high-energy electrons, while the γ -ray and optical spectra, situated before the break energy, are due to low-energy electrons. The faster cooling of high-energy electrons emitting X-rays contributes to a larger variability amplitude in the X-ray band, whereas the slower cooling of low-energy electrons results in a smaller variability amplitude in the Optical/UV and γ -ray bands.

We know that the power-law (PL) spectral shape is the characteristic feature of non-thermal emission (Landau et al., 1986). Anderhub et al. (2009) analyzed this source in a low flux state and found that the X-ray spectral shape derived from the Suzaku data from 0.6 keV to 40 keV was well described by a broken power law. However, recent observations of some blazars with sensitive Telescopes show that the X-ray spectra significantly deviate from a power-law shape and instead, they show a mild curvature in their spectra (Massaro and et al., 2008; Furniss et al., 2015; Hota et al., 2021). Our study confirms that both log-parabola and broken power law models provide a good fit to the data. Using the *AstroSat* observation, we conducted a comprehensive X-ray spectral analysis of Mrk 501. The wide-band X-ray spectrum from LAXPC and SXT instruments was jointly fitted using PL, BPL, and LP models. We noted that the PL model results in high reduced- χ^2 values compared to the BPL and LP models. However, both BPL and LP models produced similar fits with comparable reduced- χ^2 values across all observations. The hard spectrum of the source corresponds to the brightest observation considered in our work, indicating a harder brighter feature (see Figure 2). The source clearly shows a harder when brighter trend even during the low flux states. This feature is typically observed during the flaring states of blazars. In the case of LP, the spectral indices defined at the pivot energy, α ranged from 1.66 – 2.20 and the curvature parameter β ranged from 0.18 – 0.36. These values indicate that the energy spectrum of the source exhibits moderate curvature in the low flux states. Notably, the parameters

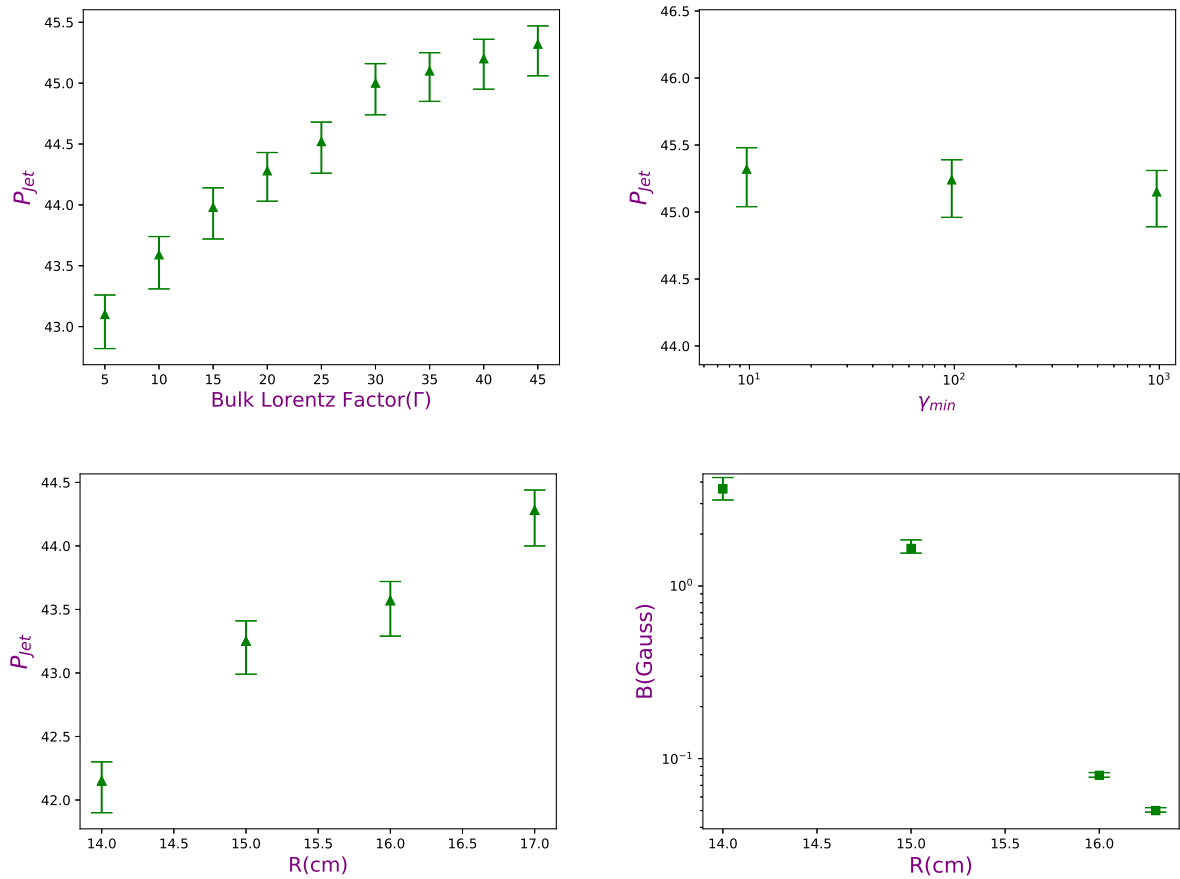


Figure 7: Jet power variation with the bulk Lorentz factor, minimum particle energy and emission region size using the LP model for the particle distribution. Top left panel is a variation of P_{jet} with Γ , top right panel is a plot of jet power with γ_{min} , the bottom left panel is a plot of P_{jet} with R . Bottom right panel represents the variation of R with a B .

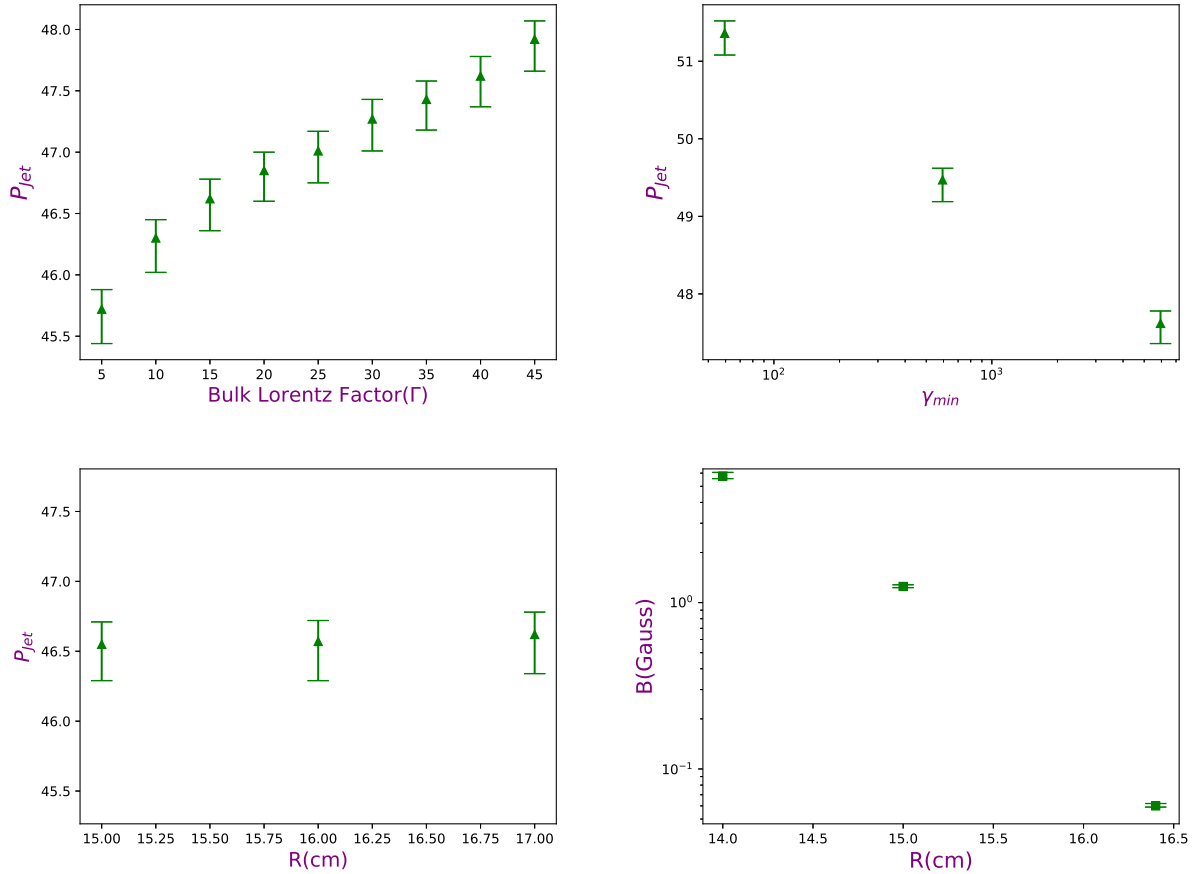


Figure 8: Jet power variation with the bulk Lorentz factor, minimum particle energy and emission region size using the BPL model for the particle distribution. The top left panel is a variation of P_{jet} with Γ , top right panel is a plot of jet power with γ_{min} , the bottom left panel is a plot of P_{jet} with R . Bottom right panel represents the variation of R with a B .

of the LP model are consistent with those of the BPL model, with the α being hardest during the bright observation. Additionally, the observation with the hardest spectrum exhibits a maximum curvature value of 0.36. The observed curvature cannot be simply attributed to the radiative cooling of high-energy electrons, such as synchrotron and inverse Compton processes. Instead, it is more likely linked to the particle distribution in the emission region resulting from stochastic acceleration, particle diffusion, or electron escape mechanisms. The standard approach to explain the curvature involves the combined effects of particle acceleration and radiative losses. For instance, (Massaro et al., 2004) demonstrated that a curved spectrum can result from an energy-dependent acceleration process, where the acceleration probability decreases with electron energy. Alternatively, an energy-dependent electron escape rate from the acceleration region can also lead to the curvature of the emitted spectrum (Jagan et al., 2018; Goswami et al., 2018). In our work, we too assumed that the intrinsically curved particle distributions are due to an energy dependence of the acceleration time-scales. However, a more comprehensive examination of the micro-physics involved in these processes is necessary to confirm the assumed dependence.

We modeled the broadband SED of Mrk 501 by using the convolved one-zone leptonic model involving the synchrotron and SSC processes. A key advantage of our model is its integration with XSPEC, allowing for rigorous statistical fitting and providing well-defined confidence intervals on the model parameters. Additionally, our code is flexible, as it can accommodate any user-defined particle distribution, including those derived from solving the Fokker-Planck equation, and easily convolve it with the broadband emission model. This provides a significant edge over other available models, where incorporating custom particle distributions can be more complex. Another important advantage is that XSPEC offers an accessible platform for constructing and customizing models, simplifying the process compared to more complex frameworks like JetSet (Tramacere et al., 2011). Additionally, while the other codes like LeHaMoC (Stathopoulos et al., 2024) and SOPRANO (Gasparyan et al., 2022) focus on modeling, they often lack the capability to provide statistical uncertainties on the parameters, whereas our method fully utilizes XSPEC's statistical fitting capabilities to ensure a more comprehensive analysis.

The Fermi-LAT γ -ray data from Mrk 501 were analysed using Fermi tools v2.2.0, following the standard procedures outlined in the Fermi-LAT documentation (Wood et al., 2017). Similarly, we processed *Swift*-UVOT into scientific products using the HEASoft packages namely *UVOT-SOURCE* and *UVOTIMSUM*. After extracting the flux points and energies, we converted them into XSPEC-compatible PHA format using the *ftflx2xsp* command. This allowed us to load the PHA files into XSPEC for the broadband spectral analysis. We considered different forms of particle distribution like BPL, LP, EDA, and ξ_{max} in our analysis for the broadband SED modelling. Initially, we freezed Γ , R, and θ at 20, 10^{17} cm and 2 degree, respectively, and varied other

parameters. We noted that the four models for the particle distribution yielded similar reduced- χ^2 values and the P_{jet} varied among the models. The P_{jet} values in units of erg/s, ranged from 43.56 - 45.10 (LP Model), 45.67 - 46.90 (BPL Model), 44.41 - 46.00 (EDA Model), and 52.60 - 54.03 (ξ_{max}). Notably, P_{jet} from the ξ_{max} model was consistently higher across observations, whereas it was comparatively lower for the LP and EDA models. Bora et al. (2024) also studied the P_{jet} of Mrk 501 during the low flux state, and similarly observed lower P_{jet} values in the LP and EDA models, with their reported ranges being 42.18 - 44.03 (LP Model), 46.6 - 48.01 (BPL Model), 42.65 - 45.06 (EDA Model), and 46.5 - 48.19 (ξ_{max} Model), which differ somewhat from our findings. Based on the criterion of minimum jet power, we excluded the ξ_{max} model as a plausible form of particle distribution responsible for the emission. Since the LP and EDA models exhibited the lowest P_{jet} , hence we chose the simpler LP model for the correlation analysis alongside the BPL model. Comparing our LP model parameters with those from Bora et al. (2024), we found that our β values (0.23 - 0.48) had a narrow range compared to the β values (0.24 - 0.79) obtained in Bora et al. (2024) work. However, the α values (2.73 - 3.62) obtained in our study were consistent with the α values (2.77 - 3.81) reported by Bora et al. (2024). In our work, the magnetic field values obtained using the LP model range from 0.003 to 0.03 G, and remain approximately 0.01 G in all flux states in the case of the BPL model.

It is important to note that TeV observations are crucial for constraining jet properties in HBLs through SED modeling. However, no simultaneous data are available for Mrk 501 during our analysis period, with the closest TeV observation separated by three months. HBLs, being low-luminosity sources with featureless spectra, are believed to scatter only synchrotron photons to high-energy γ -rays without significant contributions from external photons (Ghisellini and Tavecchio, 2008; Madejski et al., 2016). In this context, a leptonic model including synchrotron and SSC components is adequate for modeling broadband emission. Importantly, we noted that the SED parameters obtained in our work are consistent with previous results that incorporated VHE emission in the SED modeling. For example, Abdo et al. (2011) studied this source in a low flux state with VHE emission included and found broadband SED parameters, such as a magnetic field of 0.03 G and an emission region size of 10^{17} cm. In our work, we have used similar values for the broadband SED modeling. Interestingly, low values of the magnetic field are also reported in previous works (Kataoka et al., 1999; Anderhub et al., 2009; Abe et al., 2023, 2024). Additionally, Furniss et al. (2015) examined Mrk 501 in both low and high states and found that the SSC model could reproduce the observed broadband states through a decrease in magnetic field strength coupled with an increase in the luminosity and hardness of the relativistic leptons. This study also noted that the high flux state has a lower magnetic field (0.03 G) than the low flux state magnetic field (0.05 G). These studies highlight that our results remain comparable with previous studies which include VHE emission. Recently, Abe et al. (2023) used multiwavelength observations to complement IXPE pointings of Mrk 501, demonstrating that changes between different

states can be explained by variations in the magnetization of the emission region. Similarly, MAGIC Collaboration et al. (2020) noted that during the maximum X-ray activity of Mrk 501 in July 2014, the VHE γ -rays showed an elevated emission. The authors demonstrated flux variations was mainly due to changes in the break energy. These results indicate that variations in the flux of the source are mostly related to the change in the break energy and magnetic field of the emission region.

We studied the dependence of P_{jet} with Γ , γ_{\min} and R . Our study revealed a consistent increase in P_{jet} with a rise in Γ for both the models. When Γ was fixed at ~ 20 , we found that P_{jet} is independent of γ_{\min} in the case of LP model. However, in the BPL model, the P_{jet} decreased as γ_{\min} increased. Additionally, we explored the impact of R on the P_{jet} , P_{jet} increased with an increase in the values of R . While in the BPL model, P_{jet} remained constant for different values of size of the emission region. Our analysis also revealed that, in both models, the required size (R) decreased as B increased.

The comparatively low jet power acquired for the LP/EDA electron distribution models, $\sim 10^{44} \text{ erg s}^{-1}$ makes it about 10 percent of the Eddington luminosity for a $10^7 M_{\odot}$ blackhole, $L_{\text{Edd}} \sim 10^{45} \text{ erg s}^{-1}$. This implication is significant, suggesting that such a jet could be directly fueled by the accretion process. This, in turn, offers a potential framework for studying the connections between jets and accretion discs (Cao and Jiang, 1999; Ghisellini et al., 2014; Sbarato et al., 2016). Interestingly, Deng et al. (2021) also showed that for Mrk 501, the power resulting from the rotating black hole is systematically higher than the jet power, while the jet power is comparable to the power originating from the accretion disk. Moreover, previous studies have demonstrated a correlation between jet power and accretion disk luminosity (Celotti et al., 1997; Cao and Jiang, 1999; Ghisellini et al., 2014; Chen et al., 2015; Xiao et al., 2022), further supporting the connection between jet power and the accretion disk. However, it is commonly observed that in BL Lac objects, especially the HBL class, the jet power often exceeds the disk luminosity (Ghisellini et al., 2014; Goswami et al., 2024). For example, a recent study by Goswami et al. (2024) examined the behavior of various HBL sources by modeling their SEDs using three approaches and found that jet power exceeds disk luminosity for HBLs in all three methods. In these sources, the strong broad emission lines, which would typically indicate accretion disk luminosity, are generally absent. As a result, the jet power in these sources is much greater than their accretion disk luminosity (Gardner and Done, 2013). These findings suggest that the jet power could originate from the spin and mass of the central black hole. The mechanism proposed by Blandford and Znajek (1977) explains this phenomenon through the torque exerted on the rotating black hole by the magnetic field amplified by the accreting material. Thus, despite our findings, the question of what powers the jet in Mrk 501 remains unclear and warrants further investigation.

The lower jet power also implies a small energy reservoir in the jet, making it susceptible to depletion from shocks and radiative losses within a shorter time frame. Consequently, there

is a motivation for conducting a detailed investigation into the temporal evolution of a sample of blazars whose spectrum is intrinsically characterized by the curved particle distributions and hence obtain constraints on the jet power.

7. Acknowledgements

We sincerely thank the anonymous referees for their valuable feedback and suggestions, which have significantly improved the quality of our manuscript. JT, ZS and NI are thankful to the Indian Space Research Organisation, Department of Space, Government of India (ISRO-RESPOND) for the financial support. ZS is supported by the Department of Science and Technology, Govt. of India, under the INSPIRE Faculty grant (DST/INSPIRE/04/2020/002319). We express our gratitude to the Inter-University Centre for Astronomy and Astrophysics (IUCAA) in Pune, India, for the support and facilities provided.

References

- Abdo, A.A., Ackermann, M., Ajello, M., Allafort, A., Baldini, L., Ballet, J., Barbierini, G., Baring, M.G., Bastieri, D., Bechtol, K., Bellazzini, R., Berenji, B., Blandford, R.D., Bloom, E.D., Bonamente, E., Borgland, A.W., Bouvier, A., Brandt, T.J., Bregeon, J., Brez, A., Brigida, M., Bruel, P., Buehler, R., Buson, S., Caliandro, G.A., Cameron, R.A., Cannon, A., Caraveo, P.A., Carrigan, S., Casandjian, J.M., Cavazzuti, E., Cecchi, C., Charles, E., Chekhtman, A., Cheung, C.C., Chiang, J., Ciprini, S., Claus, R., Cohen-Tanugi, J., Conrad, J., Cutini, S., Dermer, C.D., de Palma, F., do Couto e Silva, E., Drell, P.S., Dubois, R., Dumora, D., Favuzzi, C., Fegan, S.J., Ferrara, E.C., Focke, W.B., Fortin, P., Frailis, M., Fuhrmann, L., Fukazawa, Y., Funk, S., Fusco, P., Gargano, F., Gasparini, D., Gehrels, N., Germani, S., Giglietto, N., Giordano, F., Girolletti, M., Glanzman, T., Godfrey, G., Grenier, I.A., Guillemot, L., Guiriec, S., Hayashida, M., Hays, E., Horan, D., Hughes, R.E., Jhannesson, G., Johnson, A.S., Johnson, W.N., Kadler, M., Kamae, T., Katagiri, H., Kataoka, J., Kndlseder, J., Kuss, M., Lande, J., Latronico, L., Lee, S.H., Lemoine-Goumard, M., Longo, F., Loparco, F., Lott, B., Lovellette, M.N., Lubrano, P., Madejski, G.M., Makkev, A., Max-Moerbeck, W., Mazziotta, M.N., McEnery, J.E., Mehault, J., Michelson, P.F., Mitthumsiri, W., Mizuno, T., Moiseev, A.A., Monte, C., Monzani, M.E., Morselli, A., Moskalenko, I.V., Murgia, S., Naumann-Godo, M., Nishino, S., Nolan, P.L., Norris, J.P., Nuss, E., Ohsugi, T., Okumura, A., Omodei, N., Orlando, E., Ormes, J.F., Paneque, D., Panetta, J.H., Parent, D., Pavlidou, V., Pearson, T.J., Pelassa, V., Pepe, M., Pesce-Rollins, M., Piron, F., Porter, T.A., Rain, S., Rando, R., Razzano, M., Readhead, A., Reimer, A., Reimer, O., Richards, J.L., Ripken, J., Ritz, S., Roth, M., Sadrozinski, H.F.W., Sanchez, D., Sander, A., Scargle, J.D., Sgr, C., Siskind, E.J., Smith, P.D., Spandre, G., Spinelli, P., Stawarz, Å., Stevenson, M., Strickman, M.S., Sokolovsky, K.V., Suson, D.J., Takahashi, H., Takahashi, T., Tanaka, T., Thayer, J.B., Thayer, J.G., Thompson, D.J., Tibaldo, L., Torres, D.F., Tosti, G., Tramacere, A., Uchiyama, Y., Usher, T.L., Vandebroucke, J., Vasileiou, V., Vilchez, N., Vitale, V., Waite, A.P., Wang, P., Wehrle, A.E., Winer, B.L., Wood, K.S., Yang, Z., Ylinen, T., Zensus, J.A., Ziegler, M., collaboration), T.F.L., Aleksic, J., Antonelli, L.A., Antoranz, P., Backes, M., Barrio, J.A., Gonzalez, J.B., Bednarek, W., Berdyugin, A., Berger, K., Bernardini, E., Biland, A., Blanch, O., Bock, R.K., Boller, A., Bonnoli, G., Bordas, P., Tridon, D.B., Bosch-Ramon, V., Bose, D., Braun, I., Bretz, T., Camara, M., Carmona, E., Carosio, A., Colin, P., Colombo, E., Contreras, J.L., Cortina, J., Covino, S., Dazzi, F., de Angelis, A., del Pozo, E.D.C., Lotto, B.D., Maria, M.D., Sabata, F.D., Mendez, C.D., Ortega, A.D., Doert, M., Dominguez, A., Prester, D.D., Dorner, D., Doro, M., Elsaesser, D., Ferenc, D., Fonseca, M.V., Font, L., Lpez, R.J.G., Garczarczyk, M., Gaug, M., Giavitto, G., Godinovi, N., Hadach, D., Herrero, A., Hildebrand, D., Hhne-Mnch, D., Hose, J., Hrupec, D., Jogler, T., Klepser, S., Krhenbhl, T., Kranich, D., Krause, J., Barbera, A.L., Leonardo, E., Lindfors, E., Lombardi, S., Lpez, M., Lorenz, E., Majumdar, P., Makariev,

- E., Maneva, G., Mankuzhiyil, N., Mannheim, K., Maraschi, L., Mariotti, M., Martnez, M., Mazin, D., Meucci, M., Miranda, J.M., Mirzoyan, R., Miyamoto, H., Moldn, J., Moralejo, A., Nieto, D., Nilsson, K., Orito, R., Oya, I., Paoletti, R., Paredes, J.M., Partini, S., Pasanen, M., Pauss, F., Pegna, R.G., Perez-Torres, M.A., Persic, M., Peruzzo, J., Pochon, J., Monroni, P.G.P., Prada, F., Prandini, E., Puchades, N., Puljak, I., Reichardt, T., Reinthal, R., Rhode, W., Rib, M., Rico, J., Rissi, M., Rgamer, S., Saggion, A., Saito, K., Saito, T.Y., Salvati, M., Snchez-Conde, M., Satalecka, K., Scalzotto, V., Scapin, V., Schultz, C., Schweizer, T., Shayduk, M., Shore, S.N., Sierpowska-Bartosik, A., Sillanp, A., Sitarek, J., Sobczynska, D., Spanier, F., Spiro, S., Stamera, A., Steinke, B., Storz, J., Strah, N., Struebig, J.C., Suric, T., Takalo, L.O., Tavecchio, F., Temnikov, P., Terzi, T., Tescaro, D., Teshima, M., Vankov, H., Wagner, R.M., Weitzel, Q., Zabalza, V., Zandanel, F., Zanin, R., collaboration), T.M., Acciari, V.A., Arlen, T., Aune, T., Benbow, W., Boltuch, D., Bradbury, S.M., Buckley, J.H., Bugaev, V., Cannon, A., Cesarini, A., Ciupik, L., Cui, W., Dickherber, R., Errando, M., Falcone, A., Finley, J.P., Finnegan, G., Fortson, L., Furniss, A., Galante, N., Gall, D., Gillanders, G.H., Godambe, S., Grube, J., Guenette, R., Gyuk, G., Hanna, D., Holder, J., Huang, D., Hui, C.M., Humensky, T.B., Kaaret, P., Karlsson, N., Kertzman, M., Kieda, D., Konopelko, A., Krawczynski, H., Krennrich, F., Lang, M.J., Maier, G., McArthur, S., McCann, A., McCutcheon, M., Moriarty, P., Mukherjee, R., Ong, R., Otte, A.N., Pandel, D., Perkins, J.S., Pichel, A., Pohl, M., Quinn, J., Ragan, K., Reyes, L.C., Reynolds, P.T., Roache, E., Rose, H.J., Rovero, A.C., Schroedter, M., Sembrroski, G.H., Senturk, G.D., Steele, D., Swordy, S.P., TeÅ, G., Theiling, M., Thibadeau, S., Varlotta, A., Vincent, S., Wakely, S.P., Ward, J.E., Weekes, T.C., Weinstein, A., Weisgarber, T., Williams, D.A., Wood, M., Zitzer, B., collaboration), T.V., Villata, M., Raiteri, C.M., Aller, H.D., Aller, M.F., Arkharov, A.A., Blinov, D.A., Calcide, P., Chen, W.P., Efimova, N.V., Kimeridze, G., Konstantinova, T.S., Kopatskaya, E.N., Koptelova, E., Kurianidze, O.M., Kurianidze, S.O., Lhteenmki, A., Larionov, V.M., Larionova, E.G., Larionova, L.V., Ligustri, R., Morozova, D.A., Nikolashvili, M.G., Sigua, L.A., Troitsky, I.S., Angelakis, E., Capalbi, M., Carramiana, A., Carrasco, L., Cassaro, P., de la Fuente, E., Gurwell, M.A., Kovalev, Y.Y., Kovalev, Y.A., Krichbaum, T.P., Krimm, H.A., Leto, P., Lister, M.L., Maccaferri, G., Moody, J.W., Mori, Y., Nestoras, I., Orlati, A., Pagani, C., Pace, C., Pearson, R., Perri, M., Piner, B.G., Pushkarev, A.B., Ros, E., Sadun, A.C., Sakamoto, T., Tornikoski, M., Yatsu, Y., Zook, A., 2011. Insights into the high-energy -ray emission of markarian 501 from extensive multifrequency observations in the fermi era. *The Astrophysical Journal* 727, 129. URL: <https://dx.doi.org/10.1088/0004-637X/727/2/129>, doi:10.1088/0004-637X/727/2/129.
- Abe, H., Abe, S., Acciari, V.A., Agudo, I., Aniello, T., Ansoldi, S., Antonelli, L.A., Arbet Engels, A., 2023. Multi-messenger characterization of mrk 501 during historically low x-ray and gamma-ray activity. *Journal Name* doi:DOI.
- Abe, S., et al., 2024. Insights into the broad-band emission of the TeV blazar Mrk 501 during the first X-ray polarization measurements arXiv:2401.08560.
- Ackermann, M., et al., 2015. Fermi-lat observations of the lmc pulsar psr j0540-6919. *The Astrophysical Journal* 807, L28.
- Agrawal, P.C., Yadav, J.S., Antia, H.M., Dedhia, D., Shah, P., Chauhan, J.V., Manchanda, R.K., Chitnis, V.R., Gujar, V.M., Katoch, T., Kurhade, V.N., Madhwani, P., Manojkumar, T.K., Nikam, V.A., Pandya, A.S., Parmar, J.V., Pawar, D.M., Roy, J., Paul, B., Pahari, M., Misra, R., Ravichandran, M.H., Anilkumar, K., Joseph, C.C., Navalgund, K.H., Pandiyani, R., Sarma, K.S., Subbarao, K., 2017. Large Area X-Ray Proportional Counter (LAXPC) Instrument on AstroSat and Some Preliminary Results from its Performance in the Orbit. *Journal of Astrophysics and Astronomy* 38, 30. doi:10.1007/s12036-017-9451-z, arXiv:1705.06446.
- Aharonian, F.A., Akhperjanian, A.G., Barrio, J.A., Bernlöhr, K., Bojahr, H., Contreras, J.L., Cortina, J., Daum, A., Deckers, T., Fonseca, V., Gonzalez, J.C., Heinzelmann, G., Hemberger, M., Hermann, G., Heß, M., Heusler, A., Hofmann, W., Hohl, H., Horns, D., Ibarra, A., Kankanyan, R., Kirstein, O., Köhler, C., Konopelko, A., Kornmeyer, H., Kranich, D., Krawczynski, H., Lampeitl, H., Lindner, A., Lorenz, E., Magnussen, N., Meyer, H., Mirzoyan, R., Moralejo, A., Padilla, L., Panter, M., Petry, D., Plaga, R., Plyasheshnikov, A., Prahl, J., Pühlhofer, G., Rauterberg, G., Renault, C., Rhode, W., Sahakian, V., Samorski, M., Schmele, D., Schröder, F., Stamm, W., Völk, H.J., Wiebel-Sooth, B., Wiedner, C., Willmer, M., Wirth, H., 1999. The temporal characteristics of the TeV gamma-radiation from MKN 501 in 1997. I. Data from the stereoscopic imaging atmospheric Cherenkov telescope system of HEGRA. *Astronomy & Astrophysics* 342, 69–86. arXiv:astro-ph/9808296.
- Ahnen, M.L., Ansoldi, S., Antonelli, L.A., Antoranz, P., Babic, A., Banerjee, B., Bangale, P., Barres de Almeida, U., Barrio, J.A., Becerra González, J., Bednarek, W., Bernardini, E., Berti, A., Biasuzzi, B., Biland, A., Blanch, O., Bonnefoy, S., Bonnoli, G., Borracci, F., Bretz, T., Buson, S., Carosi, A., Chatterjee, A., Clavero, R., Colin, P., Colombo, E., Contreras, J.L., Cortina, J., Covino, S., Da Vela, P., Dazzi, F., De Angelis, A., De Lotto, B., de Óña Wilhelmi, E., Di Pierro, F., Doert, M., Domínguez, A., Dominis Prester, D., Dorner, D., Doro, M., Einecke, S., Eisenacher Glawion, D., Elsaesser, D., Engelkemeier, M., Fallah Ramazani, V., Fernández-Barral, A., Fidalgo, D., Fonseca, M.V., Font, L., Frantzen, K., Fruck, C., Galindo, D., García López, R.J., Garczarczyk, M., Garrido Terrats, D., Gaug, M., Giannmaria, P., Godinović, N., González Muñoz, A., Gora, D., Guberman, D., Hadach, D., Hahn, A., Hanabata, Y., Hayashida, M., Herrera, J., Hose, J., Hrupec, D., Hughes, G., Idec, W., Kodani, K., Konno, Y., Kubo, H., Kushida, J., La Barbera, A., Lelas, D., Lindfors, E., Lombardi, S., Longo, F., López, M., López-Coto, R., Majumdar, P., Makariev, M., Mallot, K., Maneva, G., Mangano, M., Mannheim, K., Maraschi, L., Marcote, B., Mariotti, M., Martínez, M., Mazin, D., Menzel, U., Miranda, J.M., Mirzoyan, R., Moralejo, A., Moretti, E., Nakajima, D., Neustroev, V., Niedzwiecki, A., Nievas Rosillo, M., Nilsson, K., Nishijima, K., Noda, K., Nogués, L., Overkemping, A., Paiano, S., Palacio, J., Palatiello, M., Paneque, D., Paoletti, R., Paredes, J.M., Paredes-Fortuny, J., Pedraletti, G., Peresano, M., Perri, L., Persic, M., Poutanen, J., Prada Moroni, P.G., Prandini, E., Puljak, I., Reichardt, I., Rhode, W., Ribó, M., Rico, J., Rodriguez Garcia, J., Saito, T., Satalecka, K., Schröder, S., Schultz, C., Schweizer, T., Shore, S.N., Sillanpää, A., Sitarek, J., Snidaric, I., Sobczynska, D., Stamera, A., Steinbring, T., Strzys, M., Surić, T., Takalo, L., Tavecchio, F., Temnikov, P., Terzić, T., Tescaro, D., Teshima, M., Thaele, J., Torres, D.F., Toyama, T., Treves, A., Vanzo, G., Verguilov, V., Vovk, I., Ward, J.E., Will, M., Wu, M.H., Zanin, R., Abeysekara, A.U., Archambault, S., Archer, A., Benbow, W., Bird, R., Buchovecky, M., Buckley, J.H., Bugaev, V., Connolly, M.P., Cui, W., Dickinson, H.J., Falcone, A., Feng, Q., Finley, J.P., Fleischhacker, H., Flinders, A., Fortson, L., Gillanders, G.H., Griffin, S., Grube, J., Hütten, M., Hanna, D., Holder, J., Humensky, T.B., Kaaret, P., Kar, P., Kelley-Hoskins, N., Kertzman, M., Kieda, D., Krause, M., Krennrich, F., Lang, M.J., Maier, G., McCann, A., Moriarty, P., Mukherjee, R., Nieto, D., O'Brien, S., Ong, R.A., Otte, N., Park, N., Perkins, J., Pichel, A., Pohl, M., Popkow, A., Pueschel, E., Quinn, J., Ragan, K., Reynolds, P.T., Richards, G.T., Roache, E., Rovero, A.C., Rulten, C., Sadeh, I., Santander, M., Sembrroski, G.H., Shahinyan, K., Telezhinsky, I., Tucci, J.V., Tyler, J., Wakely, S.P., Weinstein, A., Wilcox, P., Wilhelm, A., Williams, D.A., Zitzer, B., Razzaque, S., Villata, M., Raiteri, C.M., Aller, H.D., Aller, M.F., Larionov, V.M., Arkharov, A.A., Blinov, D.A., Efimova, N.V., Grishina, T.S., Hagen-Thorn, V.A., Kopatskaya, E.N., Larionova, L.V., Larionova, E.G., Morozova, D.A., Troitsky, I.S., Ligustri, R., Calcide, P., Berdyugin, A., Kurtanidze, O.M., Nikolashvili, M.G., Kimeridze, G.N., Sigua, L.A., Kurtanidze, S.O., Chigladze, R.A., Chen, W.P., Koptelova, E., Sakamoto, T., Sadun, A.C., Moody, J.W., Pace, C., Pearson, R., Yatsu, Y., Mori, Y., Carraminya, A., Carrasco, L., de la Fuente, E., Norris, J.P., Smith, P.S., Wehrle, A., Gurwell, M.A., Zook, A., Pagani, C., Perri, M., Capalbi, M., Cesarini, A., Krimm, H.A., Kovalev, Y.Y., Kovalev, Y.A., Ros, E., Pushkarev, A.B., Lister, M.L., Sokolovsky, K.V., Kadler, M., Piner, G., Lähteenmäki, A., Tornikoski, M., Angelakis, E., Krichbaum, T.P., Nestoras, I., Fuhrmann, L., Zensus, J.A., Cassaro, P., Orlati, A., Maccaferri, G., Leto, P., Giroletti, M., Richards, J.L., Max-Moerbeck, W., Readhead, A.C.S., 2017. Multiband variability studies and novel broadband SED modeling of Mrk 501 in 2009. *Astronomy & Astrophysics* 603, A31. doi:10.1051/0004-6361/201629540, arXiv:1612.09472.
- Ahnen, M.L., Ansoldi, S., Antonelli, L.A., Arcaro, C., Babić, A., Banerjee, B., Bangale, P., Barres de Almeida, U., Barrio, J.A., Becerra González, J., Bednarek, W., Bernardini, E., Berti, A., Bhattacharyya, W., Blanch, O., Bonnoli, G., Carosi, R., Carosi, A., Chatterjee, A., Colak, S.M., Colin, P., Colombo, E., Contreras, J.L., Cortina, J., Covino, S., Cumani, P., Da Vela, P., Dazzi, F., De Angelis, A., De Lotto, B., Delfino, M., Delgado, J., Di Pierro, F., Doert, M., Domínguez, A., Dominis Prester, D., Doro, M., Eisenacher Glawion, D., Engelkemeier, M., Fallah Ramazani, V., Fernández-Barral, A., Fidalgo, D., Fonseca, M.V., Font, L., Fruck, C., Galindo, D., García López, R.J., Garczarczyk, M., Gaug, M., Giannmaria, P., Godinović, N., Gora, D., Guberman, D., Hadach, D., Hahn, A., Hassan, T., Hayashida,

- M., Herrera, J., Hose, J., Hrupec, D., Ishio, K., Konno, Y., Kubo, H., Kushida, J., Kuveždić, D., Lelas, D., Lindfors, E., Lombardi, S., Longo, F., López, M., Maggio, C., Majumdar, P., Makariev, M., Maneva, G., Manganaro, M., Maraschi, L., Mariotti, M., Martínez, M., Mazin, D., Menzel, U., Minev, M., Miranda, J.M., Mirzoyan, R., Moralejo, A., Moreno, V., Moretti, E., Nagayoshi, T., Neustroev, V., Niedzwiecki, A., Nievas Rosillo, M., Nigro, C., Nilsson, K., Ninci, D., Nishijima, K., Noda, K., Nogués, L., Paiano, S., Palacio, J., Paneque, D., Paoletti, R., Paredes, J.M., Pedalotti, G., Peresano, M., Perri, L., Persic, M., Prada Moroni, P.G., Prandini, E., Puljak, I., Garcia, J.R., Reichardt, I., Ribó, M., Rico, J., Righi, C., Rugljevac, A., Saito, T., Satalecka, K., Schroeder, S., Schweizer, T., Shore, S.N., Sitarek, J., Šnidarić, I., Sobczynska, D., Stamerra, A., Strzys, M., Surić, T., Takalo, L., Tavecchio, F., Temnikov, P., Terzić, T., Teshima, M., Torres-Albà, N., Treves, A., Tsujimoto, S., Vanzo, G., Vazquez Acosta, M., Vovk, I., Ward, J.E., Will, M., Zarić, D., Arbet-Engels, A., Baack, D., Balbo, M., Biland, A., Blank, M., Bretz, T., Bruegge, K., Bulinski, M., Buss, J., Dmytriiev, A., Dorner, D., Einecke, S., Elsaesser, D., Herbst, T., Hildebrand, D., Kortmann, L., Linhoff, L., Mahlke, M., Mannheim, K., Mueller, S.A., Neise, D., Neronov, A., Noethe, M., Oberkirch, J., Paravac, A., Rhode, W., Schleicher, B., Schulz, F., Sedlaczek, K., Shukla, A., Sliusar, V., Walter, R., Archer, A., Benbow, W., Bird, R., Brose, R., Buckley, J.H., Bugaev, V., Christiansen, J.L., Cui, W., Daniel, M.K., Falcone, A., Feng, Q., Finley, J.P., Gillanders, G.H., Gueta, O., Hanna, D., Hervet, O., Holder, J., Hughes, G., Hüttner, M., Humensky, T.B., Johnson, C.A., Kaaret, P., Kar, P., Kelley-Hoskins, N., Kertzman, M., Kieda, D., Krause, M., Krennrich, F., Kumar, S., Lang, M.J., Lin, T.T.Y., Maier, G., McArthur, S., Moriarty, P., Mukherjee, R., O'Brien, S., Ong, R.A., Otte, A.N., Park, N., Petraschik, A., Pichel, A., Pohl, M., Quinn, J., Ragan, K., Reynolds, P.T., Richards, G.T., Roache, E., Rovero, A.C., Rulten, C., Sadeh, I., Santander, M., Sembroški, G.H., Shahinyan, K., Sushch, I., Tyler, J., Wakely, S.P., Weinstein, A., Wells, R.M., Wilcox, P., Wilhel, A., Williams, D.A., Williamson, T., Zitzer, B., Perri, M., Verrecchia, F., Leto, C., Villata, M., Raiteri, C.M., Jorstad, S.G., Larionov, V.M., Blinov, D.A., Grishina, T.S., Kopatskaya, E.N., Larionova, E.G., Nikiforova, A.A., Morozova, D.A., Troitskaya, Y.V., Troitsky, I.S., Kurtanidze, O.M., Nikolashvili, M.G., Kurtanidze, S.O., Kimeridze, G.N., Chigladze, R.A., Strigachev, A., Sadun, A.C., Moody, J.W., Chen, W.P., Lin, H.C., Acosta-Pulido, J.A., Arévalo, M.J., Carnerero, M.I., González-Morales, P.A., Manilla-Robles, A., Jermak, H., Steele, I., Mundell, C., Benítez, E., Hiriart, D., Smith, P.S., Max-Moerbeck, W., Readhead, A.C.S., Richards, J.L., Hovatta, T., Lähteenmäki, A., Tornikoski, M., Tammi, J., Georganopoulos, M., Baring, M.G., 2018. Extreme HBL behavior of Markarian 501 during 2012. *Astronomy & Astrophysics* 620, A181. doi:10.1051/0004-6361/201833704, arXiv:1808.04300.
- Ajello, M., Angioni, R., Axelson, M., Ballet, J., Barbiellini, G., Bastieri, D., Becerra Gonzalez, J., Bellazzini, R., Bissaldi, E., Bloom, E.D., Bonino, R., Bottacini, E., Bruel, P., Buson, S., Carfaro, F., Cameron, R.A., Cavazzuti, E., Chen, S., Cheung, C.C., Ciprini, S., Costantin, D., Cutini, S., D'Ammando, F., de la Torre Luque, P., de Menezes, R., de Palma, F., Desai, A., Di Lalla, N., Di Venere, L., Domínguez, A., Dirirsa, F.F., Ferrara, E.C., Finke, J., Franckowiak, A., Fukazawa, Y., Funk, S., Fusco, P., Gargano, F., Garrappa, S., Gasparini, D., Giglietto, N., Giordano, F., Giroletti, M., Green, D., Grenier, I.A., Guiriec, S., Harita, S., Hays, E., Horan, D., Itoh, R., Jóhannesson, G., Kovac'evic', M., Krauss, F., Kreter, M., Kuss, M., Larsson, S., Leto, C., Li, J., Liodakis, I., Longo, F., Loparco, F., Lott, B., Lovellette, M.N., Lubrano, P., Madejski, G.M., Maldera, S., Manfreda, A., Martí-Devesa, G., Massaro, F., Mazziotta, M.N., Mereu, I., Meyer, M., Migliori, G., Mirabal, N., Mizuno, T., Monzani, M.E., Morselli, A., Moskalenko, I.V., Negro, M., Nemmen, R., Nuss, E., Ojha, L.S., Ojha, R., Omodei, N., Orienti, M., Orlando, E., Ormes, J.F., Paliya, V.S., Pei, Z., Peña-Herazo, H., Persic, M., Pesce-Rollins, M., Petrov, L., Piron, F., Poon, H., Principe, G., Rainò, S., Rando, R., Rani, B., Razzano, M., Razzaque, S., Reimer, A., Reimer, O., Schinzel, F.K., Serini, D., Sgrò, C., Siskind, E.J., Spandre, G., Spinelli, P., Suson, D.J., Tachibana, Y., Thompson, D.J., Torres, D.F., Torresi, E., Troja, E., Valverde, J., van Zyl, P., Yassine, M., 2020. The Fourth Catalog of Active Galactic Nuclei Detected by the Fermi Large Area Telescope. *The Astrophysical Journal* 892, 105. doi:10.3847/1538-4357/ab791e, arXiv:1905.10771.
- Aleksić, J., Ansoldi, S., Antonelli, L.A., Antoranz, P., Babic, A., Bangale, P., Barres de Almeida, U., Barrio, J.A., Becerra González, J., Bednarek, W., Berger, K., Bernardini, E., Biland, A., Blanch, O., Bock, R.K., Bonnefoy, S., Bonnoli, G., Borracci, F., Bretz, T., Carmona, E., Carosi, A., Carreto Fidalgo, D., Colin, P., Colombo, E., Contreras, J.L., Cortina, J., Covino, S., da Vela, P., Dazzi, F., de Angelis, A., de Caneva, G., de Lotto, B., Delgado Mendez, C., Doert, M., Domínguez, A., Dominis Prester, D., Dorner, D., Doro, M., Einecke, S., Eisenacher, D., Elsaesser, D., Farina, E., Ferenc, D., Fonseca, M.V., Font, L., Frantzen, K., Fruck, C., García López, R.J., Garczarczyk, M., Garrido Terrats, D., Gaug, M., Giavitto, G., Godinović, N., González Muñoz, A., Gozzini, S.R., Hadamek, A., Hadasch, D., Herrero, A., Hildebrand, D., Hose, J., Hrupec, D., Idec, W., Kadenius, V., Kellermann, H., Knoetig, M.L., Krause, J., Kushida, J., La Barbera, A., Lelas, D., Lewandowska, N., Lindfors, E., Lombardi, S., López, M., López-Coto, R., López-Oramas, A., Lorenz, E., Lozano, I., Makariev, M., Mallot, K., Maneva, G., Mankuzhiyil, N., Mannheim, K., Maraschi, L., Marcote, B., Mariotti, M., Martínez, M., Mazin, D., Menzel, U., Meucci, M., Miranda, J.M., Mirzoyan, R., Moralejo, A., Munar-Adrover, P., Nakajima, D., Niedzwiecki, A., Nilsson, K., Nowak, N., Orito, R., Overkemping, A., Paiano, S., Palatiello, M., Paneque, D., Paoletti, R., Paredes, J.M., Paredes-Fortuny, X., Partini, S., Persic, M., Prada, F., Prada Moroni, P.G., Prandini, E., Prezioso, S., Puljak, I., Reinthal, R., Rhode, W., Ribó, M., Rico, J., Rodriguez Garcia, J., Rügamer, S., Saggion, A., Saito, T., Saito, K., Salvati, M., Satalecka, K., Scalzotto, V., Scapin, V., Schultz, C., Schweizer, T., Shore, S.N., Sillanpää, A., Sitarek, J., Snidaric, I., Sobczynska, D., Spanier, F., Stamatescu, V., Stamerra, A., Steinbring, T., Storz, J., Sun, S., Surić, T., Takalo, L., Tavecchio, F., Temnikov, P., Terzić, T., Tescaro, D., Teshima, M., Thaele, J., Tibolla, O., Torres, D.F., Toyama, T., Treves, A., Uellenbeck, M., Vogler, P., Wagner, R.M., Zandanel, F., Zanin, R., MAGIC Collaboration, Behera, B., Beilicke, M., Benbow, W., Berger, K., Bird, R., Bouvier, A., Bugaev, B., Cerruti, M., Chen, X., Ciupik, L., Collins-Hughes, E., Cui, W., Duke, C., Dumm, J., Falcone, A., Federici, S., Feng, Q., Finley, J.P., Fortson, L., Furniss, A., Galante, N., Gillanders, G.H., Griffin, S., Griffiths, S.T., Grube, J., Gyuk, G., Hanna, D., Holder, J., Johnson, C.A., Kaaret, P., Kertzman, M., Kieda, D., Krawczynski, H., Lang, M.J., Madhavan, A.S., Maier, G., Majumdar, P., Meagher, K., Moriarty, P., Mukherjee, R., Nieto, D., O'Faoláin de Bhróithe, A., Ong, R.A., Otte, A.N., Pichel, A., Pohl, M., Popkow, A., Prokoph, H., Quinn, J., Rajotte, J., Ratliff, G., Reyes, L.C., Reynolds, P.T., Richards, G.T., Roache, E., Sembroški, G.H., Shahinyan, K., Sheidaei, F., Smith, A.W., Staszak, D., Telezhinsky, I., Theiling, M., Tyler, J., Varlotta, A., Vincent, S., Wakely, S.P., Weekes, T.C., Welsing, R., Williams, D.A., Zajczyk, A., Zitzer, B., VERITAS Collaboration, Villata, M., Raiteri, C.M., Ajello, M., Perri, M., Aller, H.D., Aller, M.F., Larionov, V.M., Efimova, N.V., Konstantinova, T.S., Kopatskaya, E.N., Chen, W.P., Koptelova, E., Hsiao, H.Y., Kurtanidze, O.M., Nikolashvili, M.G., Kimeridze, G.N., Jordan, B., Leto, P., Buemi, C.S., Trigilio, C., Umana, G., Lähteenmäki, A., Nieppola, E., Tornikoski, M., Sainio, J., Kadenius, V., Giroletti, M., Cesarini, A., Fuhrmann, L., Kovalev, Y.A., Kovalev, Y.Y., 2015. Multiwavelength observations of Mrk 501 in 2008. *Astronomy & Astrophysics* 573, A50. doi:10.1051/0004-6361/201322906, arXiv:1410.6391.
- Anderhub, H., Antonelli, L.A., Antoranz, P., Backes, M., Baixeras, C., Balestra, S., Barrio, J.A., Bastieri, D., Gonzlez, J.B., Becker, J.K., Bednarek, W., Berger, K., Bernardini, E., Biland, A., Bock, R.K., Bonnoli, G., Bordas, P., Tridon, D.B., Bosch-Ramon, V., Bose, D., Braun, I., Bretz, T., Britvitch, I., Camara, M., Carmona, E., Commichau, S., Contreras, J.L., Cortina, J., Costado, M.T., Covino, S., Curtef, V., Dazzi, F., Angelis, A.D., del Pozo, E.D.C., de los Reyes, R., Lotto, B.D., Maria, M.D., Sabata, F.D., Mendez, C.D., Dominguez, A., Dorner, D., Doro, M., Elsaesser, D., Errando, M., Ferenc, D., Fernández, E., Firpo, R., Fonseca, M.V., Font, L., Galante, N., Lpez, R.J.G., Garczarczyk, M., Gaug, M., Goebel, F., Hadasch, D., Hayashida, M., Herrero, A., Hildebrand, D., Hhne-Mnch, D., Hose, J., Hsu, C.C., Jogler, T., Kranich, D., Barbera, A.L., Laille, A., Leonardo, E., Lindfors, E., Lombardi, S., Longo, F., Lpez, M., Lorenz, E., Majumdar, P., Maneva, G., Mankuzhiyil, N., Mannheim, K., Maraschi, L., Mariotti, M., Martínez, M., Mazin, D., Meucci, M., Meyer, M., Miranda, J.M., Mirzoyan, R., Miyamoto, H., Moldn, J., Moles, M., Moralejo, A., Nieto, D., Nilsson, K., Ninkovic, J., Otte, N., Oya, I., Paoletti, R., Paredes, J.M., Pasanen, M., Pascoli, D., Pauss, F., Pegna, R.G., Perez-Torres, M.A., Persic, M., Peruzzo, L., Prada, F., Prandini, E., Puchades, N., Reichardt, I., Rhode, W., Rib, M., Rico, J., Rissi, M., Robert, A., Rgamer, S., Saggion, A., Saito, T.Y., Salvati, M., Sanchez-Conde, M., Satalecka, K., Scalzotto, V., Scapin, V., Schweizer, T., Shayduk, M., Shore, S.N., Sidro, N., Sierpowska-Bartosik, A., Sillanp, A., Sitarek, J., Sobczynska, D., Spanier, F., Stamerra, A., Stark, L.S., Takalo, L., Tavecchio, F., Temnikov, P., Tescaro, D., Teshima, M., Tluczykont, M., Torres, D.F., Turini,

- N., Vankov, H., Wagner, R.M., Wittek, W., Zabalza, V., Zandanel, F., Zanin, R., Zapatero, J., collaboration), T.M., Sato, R., Ushio, M., Kataoka, J., Madejski, G., Takahashi, T., 2009. Simultaneous multiwavelength observation of mkn 501 in a low state in 2006. *The Astrophysical Journal* 705, 1624. URL: <https://dx.doi.org/10.1088/0004-637X/705/2/1624>. doi:10.1088/0004-637X/705/2/1624.
- Atwood, W.B., Abdo, A.A., Ackermann, M., Althouse, W., Anderson, B., Axelsson, M., Baldini, L., Ballet, J., Band, D.L., Barbiellini, G., Bartelt, J., Bastieri, D., Baughman, B.M., Bechtol, K., Bédérède, D., Bellardi, F., Belazzini, R., Berenji, B., Bignami, G.F., Bisello, D., Bissaldi, E., Blandford, R.D., Bloom, E.D., Bogart, J.R., Bonamente, E., Bonnell, J., Borgland, A.W., Bouvier, A., Bregeon, J., Brez, A., Brigida, M., Bruel, P., Burnett, T.H., Busetto, G., Calandro, G.A., Cameron, R.A., Caraveo, P.A., Carius, S., Carlson, P., Casandjian, J.M., Cavazzuti, E., Ceccanti, M., Cecchi, C., Charles, E., Chekhtman, A., Cheung, C.C., Chiang, J., Chipaux, R., Cillis, A.N., Ciprini, S., Claus, R., Cohen-Tanugi, J., Condamoor, S., Conrad, J., Corbet, R., Corucci, L., Costamante, L., Cutini, S., Davis, D.S., Detocigny, D., DeKlotz, M., Dermer, C.D., de Angelis, A., Digel, S.W., do Couto e Silva, E., Drell, P.S., Dubois, R., Dumora, D., Edmonds, Y., Fabiani, D., Farnier, C., Favuzzi, C., Flath, D.L., Fleury, P., Focke, W.B., Funk, S., Fusco, P., Gargano, F., Gasparrini, D., Gehrels, N., Gentit, F.X., Germani, S., Giebels, B., Giglietto, N., Giommi, P., Giordano, F., Glanzman, T., Godfrey, G., Grenier, I.A., Grondin, M.H., Grove, J.E., Guillemot, L., Guiriec, S., Haller, G., Harding, A.K., Hart, P.A., Hays, E., Healey, S.E., Hirayama, M., Hjalmarsdotter, L., Horn, R., Hughes, R.E., Jóhannesson, G., Johansson, G., Johnson, A.S., Johnson, R.P., Johnson, T.J., Johnson, W.N., Kamae, T., Katagiri, H., Kataoka, J., Kavelaars, A., Kawai, N., Kelly, H., Kerr, M., Klamra, W., Knöldlseder, J., Kocian, M.L., Komin, N., Kuehn, F., Kuss, M., Landriu, D., Latronico, L., Lee, B., Lee, S.H., Lemoine-Goumard, M., Lionetto, A.M., Longo, F., Loparco, F., Lott, B., Lovellette, M.N., Lubrano, P., Madejski, G.M., Makeev, A., Marangelli, B., Massai, M.M., Mazzotta, M.N., McEnery, J.E., Menon, N., Meurer, C., Michelson, P.F., Minuti, M., Mirizzi, N., Mitthumsiri, W., Mizuno, T., Moiseev, A.A., Monte, C., Monzani, M.E., Moretti, E., Morselli, A., Moskalenko, I.V., Murgia, S., Nakamori, T., Nishino, S., Nolan, P.L., Norris, J.P., Nuss, E., Ohno, M., Ohsugi, T., Omodei, N., Orlando, E., Ormes, J.F., Paccagnella, A., Panequie, D., Panetta, J.H., Parent, D., Pearce, M., Pepe, M., Perazzo, A., Pesce-Rollins, M., Picozza, P., Pieri, L., Pinchera, M., Piron, F., Porter, T.A., Poupard, L., Rainò, S., Rando, R., Rapposelli, E., Razzano, M., Reimer, A., Reimer, O., Reposeur, T., Reyes, L.C., Ritz, S., Rochester, L.S., Rodriguez, A.Y., Romani, R.W., Roth, M., Russell, J.J., Ryde, F., Sabatini, S., Sadrozinski, H.F.W., Sanchez, D., Sander, A., Sapozhnikov, L., Parkinson, P.M.S., Scargle, J.D., Schalk, T.L., Scolieri, G., Sgrò, C., Share, G.H., Shaw, M., Shimokawabe, T., Shrader, C., Sierpowska-Bartosik, A., Siskind, E.J., Smith, D.A., Smith, P.D., Spandre, G., Spinelli, P., Starck, J.L., Stephens, T.E., Strickman, M.S., Strong, A.W., Suson, D.J., Tajima, H., Takahashi, H., Takahashi, T., Tanaka, T., Tenze, A., Tether, S., Thayer, J.B., Thayer, J.G., Thompson, D.J., Tibaldo, L., Tibolla, O., Torres, D.F., Tosti, G., Tramacere, A., Turri, M., Usher, T.L., Vilchez, N., Vitale, V., Wang, P., Watters, K., Winer, B.L., Wood, K.S., Ylinen, T., Ziegler, M., 2009. The Large Area Telescope on the Fermi Gamma-Ray Space Telescope Mission. *The Astrophysical Journal* 697, 1071–1102. doi:10.1088/0004-637X/697/2/1071, arXiv:0902.1089.
- Barthelmy, S.D., Barbier, L.M., Cummings, J.R., Fenimore, E.E., Gehrels, N., Hullinger, D., Krimm, H.A., Markwardt, C.B., Palmer, D.M., Parsons, A., Sato, G., Suzuki, M., Takahashi, T., Tashiro, M., Tueller, J., 2005. The Burst Alert Telescope (BAT) on the SWIFT Midex Mission. *Space Science Reviews* 120, 143–164. doi:10.1007/s11214-005-5096-3, arXiv:astro-ph/0507410.
- Blandford, R., Rees, M.J., 1978. Title of the paper. *Journal Name Volume Number, Page Range. doi:DOI*.
- Blandford, R.D., Levinson, A., 1995. Pair Cascades in Extragalactic Jets. I. Gamma Rays. *The Astrophysical Journal* 441, 79. doi:10.1086/175338.
- Blandford, R.D., Znajek, R.L., 1977. Electromagnetic extraction of energy from Kerr black holes. *Monthly Notices of the Royal Astronomical Society* 179, 433–456. URL: <https://doi.org/10.1093/mnras/179.3.433>. doi:10.1093/mnras/179.3.433, arXiv:https://academic.oup.com/mnras/article-abstract/179/3/433/1433653, mnras/179/3/433.pdf.
- Blandford, R.D., Znajek, R.L., 1977. Electromagnetic extraction of energy from Kerr black holes. *Monthly Notices of the Royal Astronomical Society* 179, 433–456. doi:10.1093/mnras/179.3.433.
- Bora, H., Khatoon, R., Misra, R., Gogoi, R., 2024. Estimating the jet power from Broadband SED modelling of Mkn 501 for different particle distributions. *Monthly Notices of the Royal Astronomical Society* 529, 4433–4441. URL: <https://doi.org/10.1093/mnras/stae706>, doi:10.1093/mnras/stae706, arXiv:https://academic.oup.com/mnras/article-abstract/529/3/4433/5814333, mnras/529/3/4433.pdf.
- Böttcher, M., Marscher, A.P., Ravasio, M., Villata, M., Raiteri, C.M., Aller, H.D., Aller, M.F., Teräsranta, H., Mang, O., Tagliaferri, G., Aharonian, F., Krawczynski, H., Kurtanidze, O.M., Nikolashvili, M.G., Ibrahimov, M.A., Papadakis, I.E., Tsinganos, K., Sadakane, K., Okada, N., Takalo, L.O., Siljanpää, A., Tosti, G., Ciprini, S., Frasca, A., Marilli, E., Robb, R., Noble, J.C., Jorstad, S.G., Hagen-Thorn, V.A., Larionov, V.M., Nesci, R., Maesano, M., Schwartz, R.D., Basler, J., Gorham, P.W., Iwamatsu, H., Kato, T., Pullen, C., Benítez, E., de Diego, J.A., Moilanen, M., Oksanen, A., Rodriguez, D., Sadun, A.C., Kelly, M., Carini, M.T., Miller, H.R., Catalano, S., Dultzin-Hacyan, D., Fan, J.H., Ghisellini, G., Ishioka, R., Karttunen, H., Keinänen, P., Kudryavtseva, N.A., Lainela, M., Lanteri, L., Larionova, E.G., Matsumoto, K., Mattox, J.R., McHardy, I., Montagni, F., Nucciarelli, G., Ostorero, L., Papamastorakis, J., Pasanen, M., Sobrito, G., Uemura, M., 2003. Coordinated Multiwavelength Observations of BL Lacertae in 2000. *The Astrophysical Journal* 596, 847–859. doi:10.1086/378156, arXiv:astro-ph/0307022.
- Burrows, D.N., Hill, J.E., Nousek, J.A., Kennea, J.A., Wells, A., Osborne, J.P., Abbey, A.F., Beardmore, A., Mukerjee, K., Short, A.D.T., Chincarini, G., Campana, S., Citterio, O., Moretti, A., Pagani, C., Tagliaferri, G., Giommi, P., Capalbi, M., Tamburelli, F., Angelini, L., Cusumano, G., Bräuning, H.W., Burkert, W., Hartner, G.D., 2005. The Swift X-Ray Telescope. *Space Science Reviews* 120, 165–195. doi:10.1007/s11214-005-5097-2, arXiv:astro-ph/0508071.
- Cao, X., Jiang, D., 1999. Link between disks and jets in radio-loud active galactic nuclei. *Publications of the Purple Mountain Observatory* 18, 243–247.
- Cao, X., Jiang, D.R., 1999. Correlation between radio and broad line emission in radio loud quasars. *Monthly Notices of the Royal Astronomical Society* 307, 802–808. URL: <https://doi.org/10.1046/j.1365-8711.1999.02657.x>, doi:10.1046/j.1365-8711.1999.02657.x, arXiv:https://academic.oup.com/mnras/article-pdf/307/4/802/1863513.pdf.
- Celotti, A., Ghisellini, G., 2008. The power of blazar jets. *Monthly Notices of the Royal Astronomical Society* 385, 283–300.
- Celotti, A., Padovani, P., Ghisellini, G., 1997. Jets and accretion processes in active galactic nuclei: further clues. *Monthly Notices of the Royal Astronomical Society* 286, 415–424. URL: <https://doi.org/10.1093/mnras/286.2.415>, doi:10.1093/mnras/286.2.415, arXiv:https://academic.oup.com/mnras/article-abstract/286/2/415/1093.mnras.2.415.pdf.
- Chen, Y.Y., Zhang, X., Xiong, D., Yu, X., 2015. Black hole mass, jet power, and accretion in agns. *The Astronomical Journal* 150, 8.
- Deng, X.C., Hu, W., Lu, F.W., Dai, B.Z., 2021. Kinetic powers of the relativistic jets in Mrk 421 and Mrk 501. *Mon. Not. Roy. Astron. Soc.* 504, 878–887. doi:10.1093/mnras/stab919, arXiv:2104.09037.
- Dermer, C.D., Schlickeiser, R., Mastichiadis, A., 1992. High-energy gamma radiation from extragalactic radio sources. *Astronomy & Astrophysics* 256, L27–L30.
- Fan, J., Kurtanidze, O., Liu, Y., et al., 2018a. Long-term multi-wavelength variability and correlation study of markarian 421 and markarian 501. *Monthly Notices of the Royal Astronomical Society* 480, 551–563. doi:10.1093/mnras/sty1867.
- Fan, J.H., Tao, J., Liu, Y., Yuan, Y.H., Sawangwit, U., Yang, J.H., Huang, Y., Zhang, Y.T., Zhang, J.Y., Zhang, L.X., Zhu, J.T., 2018b. Optical photometric monitoring for 3c 66a during 19962009 and its periodicity analysis. *The Astronomical Journal* 155, 90. URL: <https://dx.doi.org/10.3847/1538-3881/aaa547>, doi:10.3847/1538-3881/aaa547.
- Furniss, A., Noda, K., Boggs, S., Chiang, J., Christensen, F., Craig, W., Giommi, P., Hailey, C., Harisson, F., Madejski, G., Nalewajko, K., Perri, M., Stern, D., Urry, M., Verrecchia, F., Zhang, W., Team, T.N., Ahnen, M.L., Ansoldi, S., Antonelli, L.A., Antoranz, P., Babic, A., Banerjee, B., Bangale, P., de Almeida, U.B., Barrio, J.A., Gonzlez, J.B., Bednarek, W., mnras/179/3/433/1433653, mnras/179/3/433.pdf.
- G., Bonnoli, G., Borracci, F., Bretz, T., Carmona, E., Carosi, A., Chatterjee, A., Clavero, R., Colin, P., Colombo, E., Contreras, J.L., Cortina, J., Covino, S., Vela, P.D., Dazzi, F., Angelis, A.D., Caneva, G.D., Lotto, B.D., de Oa Wilhelm, E., Mendez, C.D., Pierro, F.D., Prester, D.D., Dorner, D., Doro, M., Ei-

- necke, S., Glawion, D.E., Elsaesser, D., Fernndez-Barral, A., Fidalgo, D., Fonseca, M.V., Font, L., Frantzen, K., Fruck, C., Galindo, D., Lpez, R.J.G., Garczarczyk, M., Terrats, D.G., Gaug, M., Giannmaria, P., Godinovic, N., Muoz, A.G., Guberman, D., Hanabata, Y., Hayashida, M., Herrera, J., Hose, J., Hrupec, D., Hughes, G., Idec, W., Kellermann, H., Kodani, K., Konno, Y., Kubo, H., Kushida, J., Barbera, A.L., Lelas, D., Lewandowska, N., Lindfors, E., Lombardi, S., Longo, F., Lpez, M., Lpez-Coto, R., Lpez-Oramas, A., Lorenz, E., Majumdar, P., Makariev, M., Mallot, K., Maneva, G., Managanaro, M., Mannheim, K., Maraschi, L., Marcote, B., Mariotti, M., Martnez, M., Mazin, D., Menzel, U., Miranda, J.M., Mirzoyan, R., Moralejo, A., Nakajima, D., Neustroev, V., Niedzwiecki, A., Rosillo, M.N., Nilsson, K., Nishijima, K., Orito, R., Overkemping, A., Paiano, S., Palacio, J., Palatiello, M., Paneque, D., Paoletti, R., Paredes, J.M., Paredes-Fortuny, X., Persic, M., Poutanen, J., Moroni, P.G.P., Prandini, E., Puljak, I., Reithal, R., Rhode, W., Rib, M., Rico, J., Garcia, J.R., Saito, T., Saito, K., Satalecka, K., Scapin, V., Schultz, C., Schweizer, T., Shore, S.N., Sillanp, A., Sitarek, J., Snidaric, I., Sobczynska, D., Stamer, A., Steinbring, T., Strzys, M., Takalo, L., Takami, H., Tavecchio, F., Temnikov, P., Terziec, T., Tescaro, D., Teshima, M., Thaele, J., Torres, D.F., Toyama, T., Treves, A., Verguilov, V., Vovk, I., Will, M., Zanin, R., Collaboration, T.M., Archer, A., Benbow, W., Bird, R., Biteau, J., Bugaev, V., Cardenzana, J.V., Cerutti, M., Chen, X., Ciupik, L., Connolly, M.P., Cui, W., Dickinson, H.J., Dumm, J., Eisch, J.D., Falcone, A., Feng, Q., Finley, J.P., Fleischhacker, H., Fortin, P., Fortson, L., Gerard, L., Gillanders, G.H., Griffin, S., Griffiths, S.T., Grube, J., Gyuk, G., Hkansson, N., Holder, J., Humensky, T.B., Johnson, C.A., Kaaret, P., Kertzman, M., Kieda, D., Krause, M., Krennrich, F., Lang, M.J., Lin, T.T.Y., Maier, G., McArthur, S., McCann, A., Meagher, K., Moriarty, P., Mukherjee, R., Nieto, D., de Bhrithe, A.O., Ong, R.A., Park, N., Petry, D., Pohl, M., Popkov, A., Ragan, K., Ratliff, G., Reyes, L.C., Reynolds, P.T., Richards, G.T., Roache, E., Santander, M., Sembroski, G.H., Shahinyan, K., Staszak, D., Telezhinsky, I., Tucci, J.V., Tyler, J., Vassiliev, V.V., Wakely, S.P., Weiner, O.M., Weinstein, A., Wilhelm, A., Williams, D.A., Zitzer, B., Collaboration, T.V., Vince, O., Fuhrmann, L., Angelakis, E., Karamanavis, V., Myserlis, I., Krichbaum, T.P., Zensus, J.A., Ungerechts, H., Sievers, A., Consortium, T.F.G., Bachev, R., Btcher, M., Chen, W.P., Damjanovic, G., Eswariaiah, C., Gver, T., Hovatta, T., Hughes, Z., Ibryamov, S.I., Joner, M.D., Jordan, B., Jorstad, S.G., Joshi, M., Kataoka, J., Kurtanidze, O.M., Kurtanidze, S.O., Lhteenmki, A., Latev, G., Lin, H.C., Larionov, V.M., Mokrusina, A.A., Morozova, D.A., Nikolashvili, M.G., Raiteri, C.M., Ramakrishnan, V., Readhead, A.C.R., Sadun, A.C., Sigua, L.A., Semkov, E.H., Strigachev, A., Tammi, J., Tornikoski, M., Troitskaya, Y.V., Troitsky, I.S., Villata, M., 2015. First nustar observations of mrk 501 within a radio to tev multi-instrument campaign. *The Astrophysical Journal* 812, 65. URL: <https://dx.doi.org/10.1088/0004-637X/812/1/65>, doi:10.1088/0004-637X/812/1/65.

Gardner, E., Done, C., 2013. What powers the most relativistic jets? I. BLLacs. *Monthly Notices of the Royal Astronomical Society* 438, 779–788. URL: <https://doi.org/10.1093/mnras/stt2246>, doi:10.1093/mnras/stt2246, arXiv:<https://academic.oup.com/mnras/article/438/1/779/1846057>.

Gasparyan, S., Bégué, D., Sahakyan, N., 2022. Time-dependent leptohadronic modelling of the emission from blazar jets with SOPRANO: the case of TXS 0506 + 056, 3HSP J095507.9 + 355101, and 3C 279. *Monthly Notices of the Royal Astronomical Society* 509, 2102–2121. doi:10.1093/mnras/stab2688, arXiv:[2110.01549](https://arxiv.org/abs/2110.01549).

Ghisellini, G., Tavecchio, F., 2008. The blazar sequence: a new perspective. *Monthly Notices of the Royal Astronomical Society* 387, 1669–1680. doi:10.1111/j.1365-2966.2008.13360.x, arXiv:[0802.1918](https://arxiv.org/abs/0802.1918).

Ghisellini, G., Tavecchio, F., Chiaberge, M., 2005. Structured jets in tev bl lac objects and radiogalaxies. *Astronomy and Astrophysics* 432, 401–410. doi:10.1051/0004-6361:20041404.

Ghisellini, G., Tavecchio, F., Maraschi, L., Celotti, A., Sbarrato, T., 2014. The power of relativistic jets is larger than the luminosity of their accretion disks. *Nature* 515, 376378. URL: [http://dx.doi.org/10.1038/nature13856](https://dx.doi.org/10.1038/nature13856), doi:10.1038/nature13856.

Ghisellini, G., Tavecchio, F., Maraschi, L., Celotti, A., Sbarrato, T., 2014. The power of relativistic jets is larger than the luminosity of their accretion disks. *Nature* 515, 376–378. doi:10.1038/nature13856, arXiv:[1411.5368](https://arxiv.org/abs/1411.5368).

Ghosh, P., Abramowicz, M.A., 1997. Electromagnetic extraction of rotational energy from disc-fed black holes: the strength of the Blandford-Znajek process. *Monthly Notices of the Royal Astronomical Society* 292, 887–895. doi:10.1093/mnras/292.4.887.

Gliozzi, M., Sambruna, R.M., Jung, I., Krawczynski, H., Horan, D., Tavecchio, F., 2006. Long-Term X-Ray and TeV Variability of Mrk 501. *The Astrophysical Journal* 646, 61–75. doi:10.1086/504700, arXiv:[astro-ph/0603693](https://arxiv.org/abs/astro-ph/0603693).

Goswami, P., Sahayanathan, S., Sinha, A., Misra, R., Gogoi, R., 2018. Influence of energy-dependent particle diffusion on the x-ray spectral curvature of mkn 421. *Monthly Notices of the Royal Astronomical Society* URL: [http://dx.doi.org/10.1093/mnras/sty2003](https://dx.doi.org/10.1093/mnras/sty2003), doi:10.1093/mnras/sty2003.

Goswami, P., Zacharias, M., Zech, A., Chandra, S., Boettcher, M., Sushch, I., 2024. The variety of extreme blazars in the AstroSat view. *Astronomy & Astrophysics* 682, A134. doi:10.1051/0004-6361/202348121, arXiv:[2311.12695](https://arxiv.org/abs/2311.12695).

Hota, J., Shah, Z., Khatoon, R., Misra, R., Pradhan, A.C., Gogoi, R., 2021. Understanding the X-ray spectral curvature of Mkn421 using broad-band AstroSat observations. *Mon. Not. Roy. Astron. Soc.* 508, 5921–5934. doi:10.1093/mnras/stab2903, arXiv:[2110.03344](https://arxiv.org/abs/2110.03344).

Jagan, S.K., Sahayanathan, S., Misra, R., Ravikumar, C.D., Jeena, K., 2018. Establishing the spectral turnover of blazar PKS 2155-304 as an outcome of radiative losses. *Monthly Notices of the Royal Astronomical Society: Letters* 478, L105–L109. URL: <https://doi.org/10.1093/mnrasl/sly086>, doi:10.1093/mnrasl/sly086, arXiv:<https://academic.oup.com/mnrasl/article/478/1/L105>.

Jones, T.W., O'Dell, S.L., Stein, W.A., 1974. Physics of Compact Nonthermal Sources. I. Theory of Radiation Processes. *The Astrophysical Journal* 188, 353–368. doi:10.1086/152724.

Kaastra, J.S., Bleeker, J.A.M., 2016. Astronomy 'i&' astrophysics 587, A151. doi:10.1051/0004-6361/201527616.

Kalberla, P.M.W., Burton, W.B., Hartmann, D., et al., 2005. Title of the article. *Astronomy 'i&' Astrophysics* 440, 775. doi:10.1051/0004-6361:20041864.

Kapanadze, B., Dorner, D., Romano, P., Vercellone, S., Mannheim, K., Lindfors, E., Nilsson, K., Reithal, R., Takalo, L., Kapanadze, S., Tabagari, L., 2017. The prolonged X-ray flaring activity of Mrk501 in 2014. *Monthly Notices of the Royal Astronomical Society* 469, 1655–1672. URL: <https://doi.org/10.1093/mnras/stx891>, doi:10.1093/mnras/stx891, arXiv:<https://academic.oup.com/mnras/article/469/3/1655>.

Kapanadze, B., Gurchumelia, A., Aller, M., 2023. Long-term x-ray outburst in the tev-detected blazar mrk 501 in 20212022: Further clues for the emission and unstable processes. *The Astrophysical Journal Supplement Series* 268, 20. URL: <https://dx.doi.org/10.3847/1538-4365/ace69f>, doi:10.3847/1538-4365/ace69f.

Kataoka, J., Mattox, J.R., Quinn, J., Kubo, H., Makino, F., Takahashi, T., Inoue, S., Hartman, R.C., Madejski, G.M., Sreekumar, P., Wagner, S.J., 1999. High-energy emission from the tev blazar markarian 501 during multiwavelength observations in 1996. *The Astrophysical Journal* 514, 138. URL: <https://dx.doi.org/10.1086/306918>, doi:10.1086/306918.

Landau, R., Golisch, B., Jones, T., Jones, T., Pedelty, J., Rudnick, L., Sitko, M., 2023. Active extragalactic sourcesnearly simultaneous observations from 20 centimeters to 1400 . *The Astrophysical Journal* 308, 78–92. doi:10.1086/164480.

Madejski, G.M., Nalewajko, K., Madsen, K.K., Chiang, J., Baloković, M., Paneque, D., Furniss, A.K., Hayashida, M., Urry, C.M., Sikora, M., Ajello, M., Blandford, R.D., Harrison, F.A., Sanchez, D., Giebel, B., Stern, D., Alexander, D.M., Barret, D., Boggs, S.E., Christensen, F.E., Craig, W.W., Forster, K., Giommi, P., Grefenstette, B., Hailey, C., Hornstrup, A., Kitaguchi, T., Koglin, J.E., Mao, P.H., Miyasaka, H., Mori, K., Perri, M., Pivovarov, M.J., Puccetti, S., Rana, V., Westergaard, N.J., Zhang, W.W., Zoglauer, A., 2016. First NuSTAR Observations of the BL Lac-type Blazar PKS 2155-304: Constraints on the Jet Content and Distribution of Radiating Particles. *The Astrophysical Journal* 831, 142. doi:10.3847/0004-637X/831/2/142, arXiv:[1609.02203](https://arxiv.org/abs/1609.02203).

MAGIC Collaboration, Acciari, V.A., Ansoldi, S., Antonelli, L.A., Babić, A., Banerjee, B., Barres de Almeida, U., Barrio, J.A., Becerra González, J., Bednarek, W., Bernardini, E., Berti, A., Besenrieder, J., Bhattacharyya, W., Bigongiari, C., Blanch, O., Bonoli, G., Busetto, G., Carosi, R., Ceribella, G., Cikota, S., Colak, S.M., Colin, P., Colombo, E., Contreras, J.L., Cortina, J., Covino, S., D'Elia, V., da Vela, P., Dazzi, F., de Angelis, A., de Lotto, B., Delfino, M., Delgado, J., di Pierro, F., Do Souto Espíñera, E., Domínguez, A., Dominis Prester, D., Doro, M., Fallah Ramazani, V., Fattorini, A., Fernández-Barral, A., Ferrara, G., Fidalgo, D., Foffano, L., Fonseca, M.V.,

- Font, L., Fruck, C., Galindo, D., Gallozzi, S., García López, R.J., Garczarczyk, M., Gasparyan, S., Gaug, M., Giannaria, P., Godinović, N., Guberman, D., Hadasch, D., Hahn, A., Hassan, T., Herrera, J., Hoang, J., Hrupec, D., Inoue, S., Ishio, K., Iwamura, Y., Kubo, H., Kushida, J., Kuveždić, D., Lamastra, A., Lelas, D., Leone, F., Lindfors, E., Lombardi, S., Longo, F., López, M., López-Oramas, A., Machado de Oliveira Fraga, B., Maggio, C., Majumdar, P., Makariev, M., Mallamaci, M., Maneva, G., Manganaro, M., Maraschi, L., Mariotti, M., Martínez, M., Masuda, S., Mazin, D., Minev, M., Miranda, J.M., Mirzoyan, R., Molina, E., Moralejo, A., Moreno, V., Moretti, E., Munar-Adrover, P., Neustroev, V., Niedzwiecki, A., Nievas Rosillo, M., Nigro, C., Nilsson, K., Ninci, D., Nishijima, K., Noda, K., Nogués, L., Paliano, S., Palacio, J., Paneque, D., Paoletti, R., Paredes, J.M., Pedalotti, G., Peñil, P., Peresano, M., Persic, M., Prada Moroni, P.G., Prandini, E., Puljak, I., Garcia, J.R., Ribó, M., Rico, J., Righi, C., Rugliancich, A., Saha, L., Sahayán, N., Saito, T., Satalecka, K., Schweizer, T., Sitarek, J., Šnidarić, I., Sobczynska, D., Somero, A., Stamerra, A., Strzys, M., Surić, T., Tavecchio, F., Temnikov, P., Terzić, T., Teshima, M., Torres-Albà, N., Tsujimoto, S., van Scherpenberg, J., Vanzo, G., Vazquez Acosta, M., Vovk, I., Will, M., Zarić, D., Fact Collaboration, Arbet-Engels, A., Baack, D., Balbo, M., Biland, A., Blank, M., Bretz, T., Bruegge, K., Bulinski, M., Buss, J., Doerr, M., Dorner, D., Einecke, S., Elsaesser, D., Hildebrand, D., Linhoff, L., Mannheim, K., Mueller, S., Neise, D., Neronov, A., Noethe, M., Paravac, A., Rhode, W., Schleicher, B., Schulz, F., Sedlaczek, K., Shukla, A., Sliusar, V., von Willert, E., Walter, R., Wendel, C., Tramacere, A., Lien, A., Perri, M., Verrecchia, F., Armas Padilla, M., Leto, C., Lähteenmäki, A., Tornikoski, M., Tammi, J., 2020. Study of the variable broadband emission of Markarian 501 during the most extreme Swift X-ray activity. *Astronomy & Astrophysics* 637, A86. doi:10.1051/0004-6361/201834603, arXiv:2001.07729.
- Mannheim, K., Biermann, P.L., 1992. Gamma-ray flaring of 3C 279 : a proton-initiated cascade in the jet ? *Astronomy & Astrophysics* 253, L21–L24.
- Marscher, A.P., Jorstad, S.G., D'Arcangelo, F.D., et al., 2008. The inner jet of an active galactic nucleus as revealed by a radio-to-VHE Gamma-ray outburst. *Nature* 452, 966–969. doi:10.1038/nature06895.
- Marscher, A.P., Jorstad, S.G., Morozova, D.A., et al., 2014. A new model for the inner jet of the quasar 3c 279. *The Astrophysical Journal* 780, 87. doi:10.1088/0004-637X/780/1/87.
- Massaro, E., Perri, M., Giommi, P., Nesci, R., Verrecchia, F., 2004. Intraday optical variability of radio-quiet and radio-loud quasars. *Astronomy & Astrophysics* 413, 489–499.
- Massaro, E., Perri, M., Giommi, P., Nesci, R., Verrecchia, F., 2004. Log-parabolic spectra and particle acceleration in blazars. II. The BeppoSAX wide band X-ray spectra of Mkn 501. *Astronomy & Astrophysics* 422, 103–111. doi:10.1051/0004-6361:20047148, arXiv:astro-ph/0405152.
- Massaro, F., et al., 2008. Title of the paper. *Astronomy and Astrophysics* 478, 395–400. doi:10.1051/0004-6361:20077841.
- Moderski, R., Sikora, M., 1996. On black hole evolution in active galactic nuclei. *Monthly Notices of the Royal Astronomical Society* 283, 854–864.
- Mücke, A., Protheroe, R.J., 2001. A proton synchrotron blazar model for flaring in Markarian 501. *Astroparticle Physics* 15, 121–136. doi:10.1016/S0927-6505(00)00141-9, arXiv:astro-ph/0004052.
- Padovani, P., Giommi, P., 1995. The Connection between X-Ray- and Radio-selected BL Lacertae Objects. *The Astrophysical Journal* 444, 567. doi:10.1086/175631, arXiv:astro-ph/9412073.
- Paneque, D., 2007. Study of the Flux and Spectral Variations in the VHE Emission from the Blazar Markarian 501, with the MAGIC Telescope, in: Ritz, S., Michelson, P., Meegan, C.A. (Eds.), *The First GLAST Symposium*, pp. 153–156. doi:10.1063/1.2757290, arXiv:0706.1551.
- Pian, E., Vacanti, G., Tagliaferri, G., Ghisellini, G., Maraschi, L., Treves, A., Urry, C.M., Fiore, F., Giommi, P., Palazzi, E., Chiappetti, L., Sambruna, R.M., 1998. BeppoSAX Observations of Unprecedented Synchrotron Activity in the BL Lacertae Object Markarian 501. *The Astrophysical Journal Letters* 492, L17–L20. doi:10.1086/311083, arXiv:astro-ph/9710331.
- Poole, T.S., Breeveld, A.A., Page, M.J., et al., 2008. Photometric calibration of the Swift ultraviolet/optical telescope. *Monthly Notices of the Royal Astronomical Society* 383, 627.
- Quinn, J., Akerlof, C.W., Biller, S., Buckley, J., Carter-Lewis, D.A., Cawley, M.F., Catanese, M., Connaughton, V., Fegan, D.J., Finley, J.P., Gaidos, J., Hillas, A.M., Lamb, R.C., Krennrich, F., Lessard, R., McEnery, J.E., Meyer, D.I., Mohanty, G., Rodgers, A.J., Rose, H.J., Sembroski, G., Schubnell, M.S., Weekes, T.C., Wilson, C., Zweerink, J., 1996. Detection of Gamma Rays with E_γ 300 GeV from Markarian 501. *The Astrophysical Journal Letters* 456, L83. doi:10.1086/309878.
- Rao, A.R., Bhattacharya, D., Bhalerao, V.B., Vadawale, S.V., Sreekumar, S., 2017. Cadmium-Zinc-Telluride Imager on-board AstroSat: a multi-faceted hard X-ray instrument. *Current Science* 113, 595. doi:10.18520/cs/v113/i04/595–598, arXiv:1710.10773.
- Roming, P.W.A., Kennedy, T.E., Mason, K.O., et al., 2005. Roming, P. W. A., Kennedy, T. E., Mason, K. O., & et al. *Space Science Reviews* 120, 143.
- Roy, J., Agrawal, P.C., Dedhia, D.K., Manchanda, R.K., Shah, P.B., Chitnis, V.R., Gujar, V.M., Parmar, J.V., Pawar, D.M., Kurhade, V.B., 2016. Performance of large area x-ray proportional counters in a balloon experiment. *Experimental Astronomy* 42, 249270. URL: <http://dx.doi.org/10.1007/s10686-016-9508-z>, doi:10.1007/s10686-016-9508-z.
- Rybicki, G.B., Lightman, A.P., 1986. Radiative Processes in Astrophysics.
- Sambruna, R.M., et al., 2000. A multiwavelength campaign on the tev blazar markarian 501: Implications for blazar studies with next-generation tev instruments. *The Astrophysical Journal* 538, 127–141. doi:10.1086/309108.
- Sbarato, T., Ghisellini, G., Tagliaferri, G., Perri, M., Madejski, G.M., Stern, D., Boggs, S.E., Christensen, F.E., Craig, W.W., Hailey, C.J., Harrison, F.A., Zhang, W.W., 2016. Extremes of the jetaccretion power relation of blazars, as explored by NuSTAR. *Monthly Notices of the Royal Astronomical Society* 462, 1542–1550. URL: <https://doi.org/10.1093/mnras/stw1730>, doi:10.1093/mnras/stw1730, arXiv:<https://academic.oup.com/mnras/article/462/1/1542/1680000>
- Schlafly, E.F., Finkbeiner, D.P., 2011. Measuring Reddening with Sloan Digital Sky Survey Stellar Spectra and Recalibrating SFD. *The Astrophysical Journal* 737, 103. doi:10.1088/0004-637X/737/2/103.
- Schlegel, D.J., Finkbeiner, D.P., Davis, M., 1998. Maps of Dust Infrared Emission for Use in Estimation of Reddening and Cosmic Microwave Background Radiation Foregrounds. *The Astrophysical Journal* 500, 525.
- Schleicher, B., Arbet-Engels, A., Baack, D., Balbo, M., Biland, A., Blank, M., Bretz, T., Bruegge, K., Bulinski, M., Buss, J., Doerr, M., Dorner, D., Elsaesser, D., Grischagin, S., Hildebrand, D., Linhoff, L., Mannheim, K., Mueller, S.A., Neise, D., Neronov, A., Noethe, M., Paravac, A., Rhode, W., Schulz, F., Sedlaczek, K., Shukla, A., Sliusar, V., Willert, E.v., Walter, R., 2019. Fractional Variability—A Tool to Study Blazar Variability. *Galaxies* 7, 62. doi:10.3390/galaxies7020062.
- Shah, Z., 2023. Multiwavelength variability and broad-band SED modelling of BLLac during a bright flaring period MJD5900059943. *Monthly Notices of the Royal Astronomical Society* 527, 5140–5154.
- Shah, Z., Sahayanathan, S., Mankuzhiyil, N., Kushwaha, P., Misra, R., Iqbal, N., 2017. Clues on high-energy emission mechanism from blazar 3c 454.3 during 2015 august flare. *Monthly Notices of the Royal Astronomical Society* 470, 32833299. URL: <http://dx.doi.org/10.1093/mnras/stx1194>, doi:10.1093/mnras/stx1194.
- Sikora, M., Begelman, M.C., Rees, M.J., 1994. Comptonization of Diffuse Ambient Radiation by a Relativistic Jet: The Source of Gamma Rays from Blazars? *The Astrophysical Journal* 421, 153. doi:10.1086/173633.
- Singh, K.P., Stewart, G.C., Westergaard, N.J., Bhattacharyya, S., Chandra, S., Chitnis, V.R., Dewangan, G.C., Kothare, A.T., Mirza, I.M., Mukerjee, K., Navalkar, V., Shah, H., Abbey, A.F., Beardmore, A.P., Kotak, S., Kamble, N., Vishvakarma, S., Pathare, D.P., Risbud, V.M., Koyande, J.P., Stevenson, T., Bicknell, C., Crawford, T., Hansford, G., Peters, G., Sykes, J., Agarwal, P., Sebastian, M., Rajarajan, A., Nagesh, G., Narendra, S., Ramesh, M., Rai, R., Navalagund, K.H., Sarma, K.S., Pandiyian, R., Subbarao, K., Gupta, T., Thakkar, N., Singh, A.K., Bajpai, A., 2017. Soft X-ray Focusing Telescope Aboard AstroSat: Design, Characteristics and Performance. *Journal of Astrophysics and Astronomy* 38, 29. doi:10.1007/s12036-017-9448-7.
- Stathopoulos, S.I., Petropoulou, M., Vasilopoulos, G., Mastichiadis, A., 2024. LeHaMoC: A versatile time-dependent lepto-hadronic modeling code for high-energy astrophysical sources. *Astronomy & Astrophysics* 683, A225. doi:10.1051/0004-6361/202347277, arXiv:2308.06174.
- Tandon, S.N., Hutchings, J.B., Ghosh, S.K., Subramanian, A., Koshy, G., Girish, V., Kamath, P.U., Kathiravan, S., Kumar, A., Lancelet, J.P., Madesh, P.K., Mohan, R., Murthy, J., Nagabhushana, S., Pati, A.K., Postma, J., Rao, N.K., Sankarasubramanian, K., Sreekumar, P., Sriram, S., Stalin, C.S., Sutaria, F., Sreedhar, Y.H., Barve, I.V., Mondal, C., Sahu, S., 2017. In-orbit Performance of UVIT and First Results. *Journal of Astrophysics and Astronomy* 38, 28. doi:10.1007/s12036-017-9445-x, arXiv:1612.00612.

- Tramacere, A., Massaro, E., Taylor, A.M., 2011. Stochastic Acceleration and the Evolution of Spectral Distributions in Synchro-Self-Compton Sources: A Self-consistent Modeling of Blazars' Flares. *The Astrophysical Journal* 739, 66. doi:10.1088/0004-637X/739/2/66, arXiv:1107.1879.
- Urry, C.M., Mushotzky, R.F., 1982. PKS 2155-304 : relativistically beamed synchrotron radiation from a BL Lacertae object. *The Astrophysical Journal* 253, 38–46. doi:10.1086/159607.
- Urry, C.M., Padovani, P., 1995. Unified Schemes for Radio-Loud Active Galactic Nuclei. *Publications of the Astronomical Society of the Pacific* 107, 803. doi:10.1086/133630, arXiv:astro-ph/9506063.
- Vaughan, S., Edelson, R., Warwick, R.S., Uttley, P., 2003. On characterizing the variability properties of X-ray light curves from active galaxies. *Monthly Notices of the Royal Astronomical Society* 345, 1271–1284. doi:10.1046/j.1365-2966.2003.07042.x, arXiv:astro-ph/0307420.
- Wills, B.J., Wills, D., Breger, M.J., 1992. Are the broad emission line regions in seyfert 1 galaxies really stable? *The Astrophysical Journal* 398, 454–469. doi:10.1086/171876.
- Wood, M., Caputo, R., Charles, E., Di Mauro, M., Magill, J., Perkins, J.S., Fermi-LAT Collaboration, 2017. Fermipy: An open-source Python package for analysis of Fermi-LAT Data, in: 35th International Cosmic Ray Conference (ICRC2017), p. 824. doi:10.22323/1.301.0824, arXiv:1707.09851.
- Xiao, H., Ouyang, Z., Zhang, L., Fu, L., Zhang, S., Zeng, X., Fan, J., 2022. The relativistic jet and central engine of fermi blazars. *The Astrophysical Journal* 925, 40. URL: <https://dx.doi.org/10.3847/1538-4357/ac36da>, doi:10.3847/1538-4357/ac36da.
- Yadav, J.S., Agrawal, P.C., Antia, H.M., Chauhan, J.V., Dedhia, D., Katoch, T., Madhwani, P., Manchanda, R.K., Misra, R., Pahari, M., Paul, B., Shah, P., 2016. Large Area X-ray Proportional Counter (LAXPC) instrument onboard ASTROSAT, in: den Herder, J.W.A., Takahashi, T., Bautz, M. (Eds.), Space Telescopes and Instrumentation 2016: Ultraviolet to Gamma Ray, p. 99051D. doi:10.1117/12.2231857.
- Zhang, H., Böttcher, M., 2013. X-Ray and Gamma-Ray Polarization in Leptonic and Hadronic Jet Models of Blazars. *The Astrophysical Journal* 774, 18. doi:10.1088/0004-637X/774/1/18, arXiv:1307.4187.
- Zhang, H., Chen, X., Böttcher, M., 2014. Synchrotron Polarization in Blazars. *The Astrophysical Journal* 789, 66. doi:10.1088/0004-637X/789/1/66, arXiv:1401.7138.
- Zhang, Z., Gupta, A.C., Gaur, H., Wiita, P.J., An, T., Lu, Y., Fan, S., Xu, H., 2021. X-ray intraday variability of the tev blazar pks 2155304 with suzaku during 20052014. *The Astrophysical Journal* 909, 103. URL: <https://dx.doi.org/10.3847/1538-4357/abdd38>, doi:10.3847/1538-4357/abdd38.